Optical properties of single-crystal $La_2CuO_{4+\delta}$

M. A. Quijada* and D. B. Tanner
Department of Physics, University of Florida, Gainesville, Florida 32611

F. C. Chou† and D. C. Johnston
Ames Laboratory and Department of Physics and Astronomy, Iowa State University, Ames, Iowa 50011

S.-W. Cheong
AT&T Bell Laboratories, Murray Hill, New Jersey 07974
(Received 30 May 1995)

The c-axis and ab-plane optical reflectance of an electrochemically oxidized single crystal of $La_2CuO_{4+\delta}$ ($T_c \sim 40$ K; $\delta \sim 0.12$) have been measured over a wide frequency range (30–40 000 cm^{-1}) and at temperatures between 10 and 300 K. The ab-plane optical conductivity shows metallic behavior at low frequency with weak phonon features whereas the c-axis spectrum is typical of an insulator, showing only phonons. Estimates of the carrier density and the oxygen concentration suggest that each excess oxygen contributes just over one mobile hole. The ab-plane midinfrared conductivity obtained when the wave vector $\mathbf{q}$ of the light is perpendicular to the CuO_2 planes in the sample exhibits structure that is absent when $\mathbf{q}$ is parallel to the basal planes. The ab-plane conductivity shows a strong departure from Drude metallic response; fits to midinfrared models with frequency-dependent damping require also an additional bound-carrier contribution. A superconducting condensate is evident in the low-frequency ab-plane data; the oscillator strength of this condensate contains about 18% of the doping induced or 80% of the free carrier spectral weight in the normal state. Finally, an anomalous temperature dependence is found in the visible/ultraviolet region of the spectrum.

I. INTRODUCTION

Optical absorption studies of the stoichiometric compound La_2CuO_4 have revealed it to be a charge transfer insulator having marked anisotropy in both phonon and electronic features as the polarization of the light is oriented parallel and perpendicular to the CuO_2 planes.[1–7] Most optical investigations of superconducting materials derived from this parent compound have been for the Sr-doped $La_{2-x}Sr_xCuO_4$.[3,7–10] The strong anisotropy that is present between the in-plane and out-of-plane optical properties of Sr-doped samples became evident as soon as the first polarized studies of single-crystal samples were performed.[1–3,8] In one of the early reports,[3] the reflectance of insulating La_2CuO_4 and of 8% Sr-doped samples was compared for polarizations parallel and perpendicular to the CuO_2 planes. The c-axis reflectance in both cases is virtually the same, suggesting that doping does not affect the c-axis optical properties of the system. (In this paper, we call the axis perpendicular to the CuO_2 planes the c axis and use a tetragonal classification for the phonon modes.) The spectra are typical of an insulating material, with phonon structure due to infrared-active modes (A_{2u} symmetry). In contrast, the reflectance parallel to the ab planes shows substantial changes with doping. The undoped sample has a reflectance that is dominated by infrared-allowed phonons (E_u symmetry) and constant low-frequency reflectance, indicative of insulating behavior for electric field parallel to the CuO_2 planes. The doped sample shows a reflectance rising as $\omega \rightarrow 0$, with the phonon structure greatly reduced due to screening by the free carriers. This reflectance implies a metallic conductivity in the CuO_2 planes of this doped material, although the sample studied was not superconducting. It became clear from this study that the anisotropy between the ab-plane and the c-axis optical conductivity of the doped sample would make it very difficult to interpret the results that were first observed in unaligned samples.[11–13]

A systematic study of the c-axis and ab-plane optical properties as a function of Sr doping in $La_{2-x}Sr_xCuO_4$ was done by Uchida *et al.*[8] These results confirmed the previous observation that the c-axis spectrum, dominated by two major optical phonons, is almost unchanged between the insulating and the doped phases. Only in the overdoped, nonsuperconducting samples were there qualitative changes in the reflectance. In this case, the spectrum appeared to have a free-carrier component, although the highest-frequency phonon was not completely screened. This observation is consistent with a quasimetallic behavior in the c-axis resistivity as a function of temperature at this concentration.[8] In this context, the overdoped samples are regarded as anisotropic three-dimensional metals.

The temperature dependence of the c-axis optical properties of $La_{2-x}Sr_xCuO_4$ has been investigated by Tamasaku *et al.*[9] Above T_c, the far-infrared reflectance is rather featureless, approaching a constant value at low frequencies for the lowest doping, and showing a slight negative slope for higher doping. The latter behavior is indicative of some free-carrier behavior. Below T_c, a sharp edge develops in the reflectance, signaling the onset of superconductivity. This edge does not scale with T_c and it is not due to a superconducting gap excitation, but rather to a plasma-edge-like feature of the superconducting-state carriers.

The ab-plane response shows marked change with doping.[8] At low doping levels, there is evidence of a midin-

0163-1829/95/52(21)/15485(19)/$06.00

frared component to the real part of the optical conductivity, $\sigma_1(\omega)$, in addition to the free-carrier response at low frequencies. In lightly Sr-doped samples ($x=0.02$), the maximum of this midinfrared mode is around 0.5 eV (4000 cm^{-1}), while for a doping level of $x=0.1$ the maximum appears at 0.14 eV (1100 cm^{-1}). The presence of these optical excitations has also been established in studies of lightly oxygen-doped $La_2CuO_{4+\delta}$ single crystals.[7,14]

The temperature dependence of the ab-plane optical properties of a $La_{2-x}Sr_xCuO_4$ film ($x=0.17$) was investigated by Gao *et al.*[10] Analysis of the data within the framework of a two-component picture indicates the normal-state free-carrier component of the conductivity has a scattering rate that is linear in temperature and an oscillator strength that is nearly temperature independent. By contrast, the midinfrared conductivity shows a much weaker temperature dependence. In the superconducting state, 85% of the free-carrier oscillator strength condenses into the superfluid condensate: a δ function at $\omega=0$.

In contrast to the case of cation doped $La_{2-x}Sr_xCuO_4$, relatively few optical studies of anion-doped compounds such as $La_2CuO_{4+\delta}$ have been made. The T-δ phase diagram of the latter system[15,16] is significantly different from the T-x phase diagram of the Sr-doped material.[17] The $\delta=0$ endmember is an antiferromagnetic insulator with a Néel temperature $T_N\simeq 325$ K. With increasing δ, T_N decreases, reaching 250 K at $\delta\simeq 0.012$. Between this composition and $\delta\simeq 0.06$, both antiferromagnetism (with a 250 K T_N) and superconductivity with $T_c\simeq 34$ K are observed. This behavior is on account of phase separation associated with a miscibility gap in the low-temperature phase diagram for $0.01\lesssim\delta\lesssim 0.06$.[15,16] Spin-glass behavior, such as occurs at low doping levels in $La_{2-x}Sr_xCuO_4$, is not found in the oxygen rich samples.[17–19]

In samples with oxygen contents just at the oxygen-rich miscibility-gap boundary, a single phase, with $T_c\simeq 34$ K is found.[16] These superconducting samples do not exhibit phase separation or changes in the average unit cell symmetry below room temperature.[20] As δ increases further to $\delta\simeq 0.12$, another phase (or phases) with $T_c\simeq 40$–45 K is found.[16,20]

The excess oxygen atoms in the oxygen-rich phase(s) are located between adjacent La layers, coordinated by four La atoms;[20,21] these positions are the same as those of the out-of-plane oxygen atoms in the so-called T' structure of Nd_2CuO_4. The single-phase compositions with $\delta>0.06$ are known to have an orthorhombic cell,[20–22] but the space-group symmetry of this cell is controversial. Jorgensen and coworkers[20,22] assert that the space group is $Fmmm$ whereas Chaillout *et al.*[21] believe that it is $Cmca$ as in undoped La_2CuO_4 below the 530 K tetragonal to orthorhombic transformation. This difference in space group assignment has led to differing views of how the apical oxygen positions are distorted by the excess oxygen atoms. An additional complication is that both neutron diffraction[20] and transmission electron microscopy[23,24] measurements exhibit superstructure reflections, presumably associated with ordering of the excess oxygen atoms. The details of the temperature and compositional dependence of this ordering, its effects on T_c, and its influence on other physical properties are unclear at present.

The number of holes, p, doped into the CuO_2 plane in $La_2CuO_{4+\delta}$ by each excess oxygen atom is presently an open issue. Some previous work on this problem[16,20,25] indicates that for the $\delta\simeq 0.06$ phase with $T_c\simeq 34$ K, each excess oxygen contributes about one hole, ($p/\delta\sim 1$) whereas for the phase(s) with $T_c\simeq 40$–45 K, $p/\delta\sim 1.5$. In contrast, other investigators[26] believe that $p/\delta=2$ for all δ.

In this paper, we report the optical properties of an oxygen-doped $La_2CuO_{4+\delta}$ single crystal ($\delta\sim 0.12$). In principle, optical studies can shed light on all three of the above issues, i.e., the nature of the detailed structure, the temperature dependence of the superlattice ordering, and the doped hole concentration p. We studied the optical properties of our oxygen-doped sample by measuring the reflectance of light polarized along the c axis and the ab plane. As in the undoped material, the spectrum along the c direction is mainly dominated by optical phonons and no evidence of metallic component is found in the optical conductivity. The mode at 500 cm^{-1}, assigned to the stretching motion of the apical oxygens, is split into two modes in the oxygen-doped sample, implying that the motion of these oxygen atoms is strongly affected by the insertion of extra oxygen.

The ab-plane response shows metallic reflectance in the far infrared and a plasma edge around $\omega\sim 7500$ cm^{-1}. Kramers-Kronig analysis of the ab-plane reflectance reveals the unusual non-Drude behavior in the midinfrared conductivity that is typical of the copper-oxide superconductors. In addition, for frequencies in the near infrared and above, a rather unusual temperature dependence is observed in the optical reflectance of the sample. There is a sharpening of the plasma edge at 7500 cm^{-1}, as expected, but there is also a gradual decrease in reflectance as the temperature of the sample is lowered. This result suggests a temperature dependence to some high-frequency interband transition. A similar temperature dependence has been reported in Sr-doped and lightly oxygen-doped samples.[10,14]

The far-infrared conductivity is consistent with the dc conductivity,[27] increasing as temperature is lowered. The width of the zero-frequency peak also narrows at lower temperatures. Below T_c, most of the oscillator strength associated with this low-frequency response goes into the zero-frequency δ-function conductivity of the superconductor. Although the condensate contribution is evident in our measurements, there is no feature that can be identified as the superconducting gap in our data.

Finally, a comparison of the ab-plane reflectance measured from two faces of the sample, one where the wave vector $\mathbf{q}$ of the light is parallel to c and one where it is perpendicular to c, reveals some interesting features. In the first case, the ab-plane response displays some structure in the infrared region that is not present when the reflectance is measured with $\mathbf{q}\perp c$. A comparison of the sum rule in the two cases reveals that the differences in the spectra are not due to different oxygen compositions in the two surfaces of the sample. As was first pointed out by Reedyk *et al.*,[28] the differences are most likely due to electron-phonon interactions that are enhanced when the wave vector of the incident light is parallel to the c axis.

II. EXPERIMENT

Our sample was prepared by electrochemical insertion of oxygen into La_2CuO_4. Normally, oxygen addition in this ma-

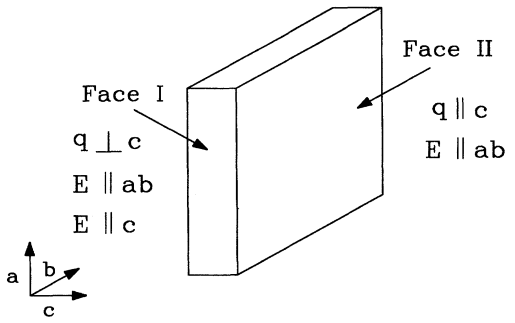

FIG. 1. Sketch of the sample showing the faces that were used to measure the reflectance of the $La_2CuO_{4+\delta}$ single crystal.

terial is obtained by annealing the sample at high temperatures (~500 °C) in an oxygen-rich environment.[29,30] As mentioned above, there are a few drawbacks in producing $La_2CuO_{4+\delta}$ samples using this method. In the first place, there is the requirement for extremely high oxygen partial pressures (~25 kbar) in order to produce fully superconducting samples ($\delta \gtrsim 0.06$). Secondly, at lower oxygen concentrations, the material tends to phase separate into oxygen-rich and oxygen-poor regions, a result of a miscibility gap[15] with boundaries $0.01 \lesssim \delta \lesssim 0.06$ below 200 K. Difficulties in producing uniformly oxidized samples could be one of the reasons why reports of optical measurements of oxygen-doped samples have been limited to lightly-doped, nonsuperconducting samples.[4,7,14]

Recent developments in electrochemical techniques have made possible the synthesis of uniformly oxidized samples with relatively high oxygen content ($\delta \sim 0.12$) and transition temperatures near 40 K.[31,32] The process of synthesizing our crystal of $La_2CuO_{4+\delta}$ began with a single crystal of La_2CuO_4, prepared using a self-flux method.[33] The oxidation of this crystal was carried out using an electrochemical cell with the La_2CuO_4 sample as the working electrode.[27,32] A platinum wire was attached to one side of the crystal using silver paint and the contact was fully covered with silicone rubber. The configuration of the electrochemical cell was La_2CuO_4/1*N* NaOH/Pt. The cell was charged by applying an anodic current of 10 μA to the La_2CuO_4 crystal for a period of two months. The exact oxygen content of the sample after the oxidation was completed is not known. Calculations based on the weight change could not be used because small pieces of the crystal were lost during handling. Meissner effect data indicate an onset of superconductivity at around 40 K.[27] A comparison of this with the onset of other samples of known oxygen concentration suggests that the excess oxygen content is around $\delta \sim 0.12$. This crystal was denoted "Crystal B" in Ref. 27, and further characterization can be found there. The resistivity of this sample was not measured, but that of a similar sample[27] was found to be "metallic" in nature. The *c*-axis resistivity was $\approx$300 mΩ-cm and nearly *T* independent. The *ab*-plane resistivity was relatively large, 2.5 mΩ-cm at 300 K, decreasing to 1 mΩ-cm at 50 K.

The frequency-dependent reflectance was measured at near-normal incidence. The reflectance was measured from two faces of the crystal. One of the faces (the face labeled I in Fig. 1) contained both the *c*-axis and either the *a*- or *b*-axis direction. (On account of twinning, we were unable to distinguish between these two directions.) Face I allowed us to use linearly polarized light to probe the optical response of the *c* axis [001] as well as the *ab*-plane response. The far-infrared and midinfrared spectral regions (50–3000 cm^{-1}) were measured at several temperatures above and below the superconducting transition temperature, while higher frequencies were only measured at 300 K. The second face that was measured, face II in Fig. 1, provided another measure of the *ab*-plane response. In this case, the optical reflectance was measured in a frequency range that extended from the far-infrared to the near-ultraviolet spectral regions (80–38 000 cm^{-1}). Temperature dependent measurements, above and below T_c, were also carried out in the same range of frequencies.

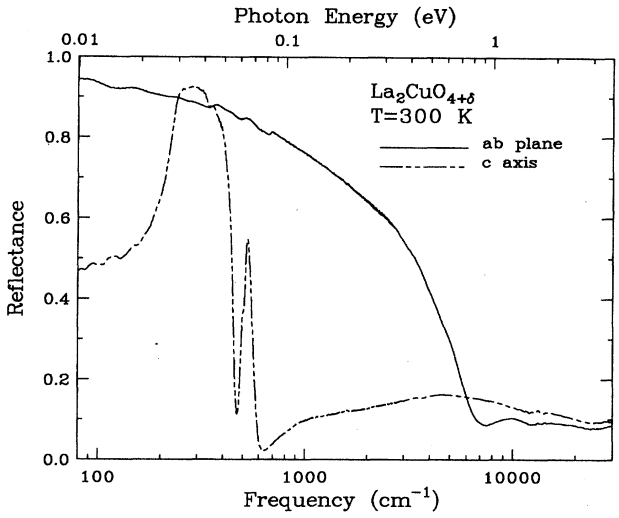

FIG. 2. Reflectance of the $La_2CuO_{4+\delta}$ single crystal (face I) for light polarized along the *ab* plane and the *c* axis (T=300 K).

A Perkin-Elmer 16U grating spectrometer was used in the near-infrared to ultraviolet regions. The far-infrared and midinfrared regions were covered using a Bruker IFS 113v Fourier transform spectrometer. The temperature of the sample was varied by using a flow cryostat with a calibrated Si-diode thermometer mounted nearby. Determination of the absolute value of the reflectance was done by coating the sample with a 2000 Å film of Al after measuring the uncoated sample. The spectra of the uncoated sample were then divided by the obtained spectrum of the coated sample and corrected for the known reflectance of Al. The accuracy in the absolute reflectance is estimated to be $\pm 1\%$.

III. ROOM-TEMPERATURE SPECTRA

Figure 2 shows the room-temperature reflectance for light polarized parallel and perpendicular to the *c* axis of the sample. This spectrum was taken on face I of the crystal. The results show a dramatic anisotropy for the in-plane and out-of-plane optical properties, as has been reported in Sr-doped superconducting samples.[3,7,8,34]

The *c*-axis reflectance has the character of an insulator at low frequencies. This reflectance is dominated by optical

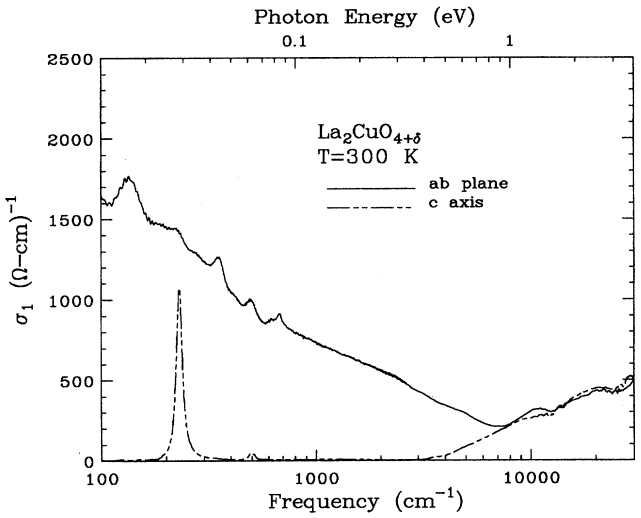

FIG. 3. Room-temperature optical conductivity $\sigma_1(\omega)$ for two polarizations obtained from a Kramers-Kronig analysis of the room-temperature reflectance.

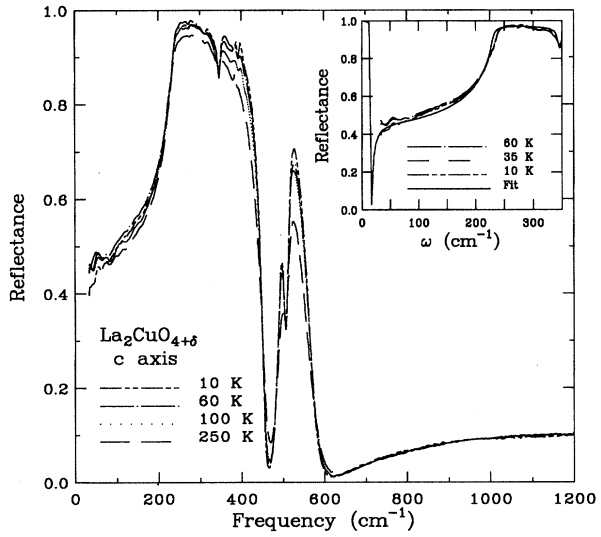

FIG. 4. Temperature dependence of the c-axis reflectance of the $La_2CuO_{4+\delta}$ single crystal. Inset: Low-frquency reflectance, with fit described in the text.

phonons in the far infrared. For higher frequencies, the spectrum is almost featureless, showing only a broad electronic feature whose maximum is around $\omega \sim 4500$ cm^{-1}. The spectrum is very similar to the c-axis spectrum of the undoped material. However, there is a weak structure that appears just below the peak of the phonon mode at 512 cm^{-1}. This structure, which is not present in the stoichiometric material,[1,3] is resolved as an additional phonon mode as the temperature of the sample is lowered.

The reflectance for polarization of the electric field parallel to the CuO_2 plane is also shown in Fig. 2. There is a marked contrast for polarization of the light parallel and perpendicular to CuO_2 planes. The ab-plane spectrum exhibits metallic behavior at low frequencies. Weak phonon modes, which are not completely screened by the free carriers in the CuO_2 planes, are also visible in the far infrared. At higher frequencies, we observe a plasma edge, with a minimum at $\omega \sim 7500$ cm^{-1}. This energy is not much different than the one observed in Sr-doped superconducting samples.[7,8] For frequencies above the plasmon minimum, we see the usual charge transfer (CT) peak at $\omega \sim 11\,500$ cm^{-1}, followed by higher energy interband transitions.

The real part of the conductivity, $\sigma_1(\omega)$, obtained from a Kramers-Kronig analysis of the reflectance,[35] is shown in Fig. 3. The usual requirement of the Kramers-Kronig integrals to extend the reflectance at the low- and high-frequency ends was done in the following way. At low frequencies, the ab-plane extension was done by modeling the reflectance using a Drude-Lorentz model and using the fitted results to extend the reflectance below the lowest frequency measured in the experiment. The c-axis reflectance was taken as constant below the lowest measured frequency. The high-frequency extrapolations were done by merging the data, which only extend up to 38 000 cm^{-1} (4.7 eV), with the results of Tajima *et al.*,[36] which extend up to 40 eV. For the ab-plane data we used the results for Sr-doped samples in Ref. 36. The range beyond 40 eV was extended with a power law $R \sim \omega^{-4}$, which is the free-electron behavior limit. More details are given in Sec. V C.

In the conductivity spectra of Fig. 3 the phonon modes and the electronic features are more easily seen. The results presented here indicate that oxygen doping in the lanthanum cuprate mostly affects the electronic excitations related to the copper-oxide planes in the system. Similar conclusions regarding the quasi-two-dimensional nature of the electronic properties in the copper-oxide superconductors have also been drawn from measurements of $YBa_2Cu_3O_{7-\delta}$ and $Bi_2Sr_2CaCu_2O_8$ materials.[37–40]

IV. c-AXIS SPECTRA

A. Temperature dependence of the c-axis reflectance

Figure 4 displays the c-axis reflectance in the infrared region at four temperatures. As the sample is cooled, the phonon lines become sharper, as expected. The structure that appears in the room-temperature spectrum just below 512 cm^{-1} is more clearly resolved as a phonon mode at 492 cm^{-1}. As mentioned before, this is not present in the c-axis spectrum of either undoped or Sr-doped samples.[1,3]

At low frequencies, we notice that all spectra above T_c approach a constant value for the reflectance. The absence of low-frequency dispersion in $R(\omega)$ suggests that $\epsilon_1(\omega) \simeq \epsilon_1(0)$, and that there is minimal response from free carriers. From the low-frequency value of $R \simeq 0.46$, we obtain $\epsilon_1(0) \simeq 27$. This value is in excellent agreement with the "high frequency" (10^7 Hz) results of Chen *et al.*[41] for La_2CuO_4, as well as the c-axis dielectric constant from infrared reflectance reported by Collins *et al.*[3] The "optical" dielectric constant can be estimated from the midinfrared reflectance of $R \simeq 0.10$ to be $\epsilon_{1\text{opt}} \simeq 3.7$. The difference between these two numbers illustrates the large lattice polarizibility of La_2CuO_4.

In contrast to the insulating behavior in the normal state, the data at the lowest temperature show a downward trend

towards low frequencies that is not present above T_c. This trend is most likely correlated with the appearance of a minimum below 30 cm^{-1} in the superconducting-state reflectance, as was observed in the c-axis spectrum of $La_{2-x}Sr_xCuO_4$ by Tamasaku *et al.*[9] In that study, the minimum is a plasmon brought on by the formation of a superfluid condensate. A formula that accounts for the contribution of this condensate to the dielectric function in the low-frequency region is[42,43]

$$\epsilon(\omega) = -\frac{\omega_{ps}^2}{\omega(\omega + i0^+)} + \epsilon_1(0), \tag{1}$$

where ω_{ps} represents the oscillator strength of the superconducting condensate, $i0^+$ is the scattering rate that tends to zero as the the quasiparticle lifetime becomes infinite in the superconducting state, and $\epsilon_1(0)$ the dielectric constant from the optical phonons and interband transitions. Equation (1) represents the contribution of a condensate that gives a δ-function peak in $\sigma_1(\omega)$ at $\omega=0$. Doping studies[9] suggest that the reflectance edge associated with this condensate moves toward lower frequencies as the doping level in the sample is decreased, as expected. The inset to Fig. 4 shows a fit to our low-temperature data using a dielectric function model that includes Eq. (1) along with Lorentzian terms for the phonons. (See the following section for details of the fit.) In order to fit this edge in our data, we used a condensate oscillator strength of $\omega_{ps} \sim 85$ cm^{-1}. A comparison of this value with the results presented by Tamasaku *et al.*[9] for Sr-doped samples puts the effective carrier doping in our sample at $p \sim 0.11$. [Note that ω_{ps} is the unscreened plasma frequency; the reflectance minimum occurs near the screened plasma frequency $\omega_{ps}/\sqrt{\epsilon_1(0)} \simeq 20$ cm^{-1}.] On account of the sample size, the lowest frequency measured in the present experiment was around 33 cm^{-1}, so that the plasma edge was not observed.

B. Assignment of the c-axis phonons

Let us turn our attention to a quantitative analysis of the phonon modes shown in Fig. 4. In order to perform a Kramers-Kronig analysis, the normal-state reflectance at the low-frequency end was kept constant, as is customary for insulators. Below T_c the positive slope of $R(\omega)$ at low frequencies required us to use Eq. (1) as a low-frequency extension.

The results of the Kramers-Kronig analysis are shown in Figs. 5 and 6. The top panel of Fig. 5 shows the real part of the optical conductivity, $\sigma_1(\omega)$, while the bottom panel shows the energy loss function, $-\mathrm{Im}(1/\epsilon)$. Figure 6 shows the real part of the dielectric function ϵ_1. This analysis reveals that the c-axis conductivity is dominated by a total of four infrared-active modes centered at 230, 340, 492, and 512 cm^{-1}. A comparison of these frequencies with other optical studies[1,3,7] of the c-axis spectrum in undoped and Sr-doped samples of La_2CuO_4 indicates good agreement with the first two phonon modes. However, in those studies only one mode is observed at ~ 501 cm^{-1}. Group theoretical analyses[44,45] indicate that modes of ionic displacements ($\mathbf{q}=0$) along the c axis in the nearly tetragonal structure of $La_2CuO_{4+\delta}$ will have the A_{2u} symmetry. In particular, calculations of the eigenfrequencies by Mostoller *et al.*,[44] using a shell model in the undoped unit cell, give modes with A_{2u} symmetry at 242, 361, and 491 cm^{-1}. The eigenvector for the latter mode at 491 cm^{-1} involves in-phase vibrations of the apical oxygens along c with respect to the four oxygen atoms in the plane. Based on this, the present data suggest that the splitting into two modes at 492 and 512 cm^{-1} is most likely associated with the incorporation of additional oxygen

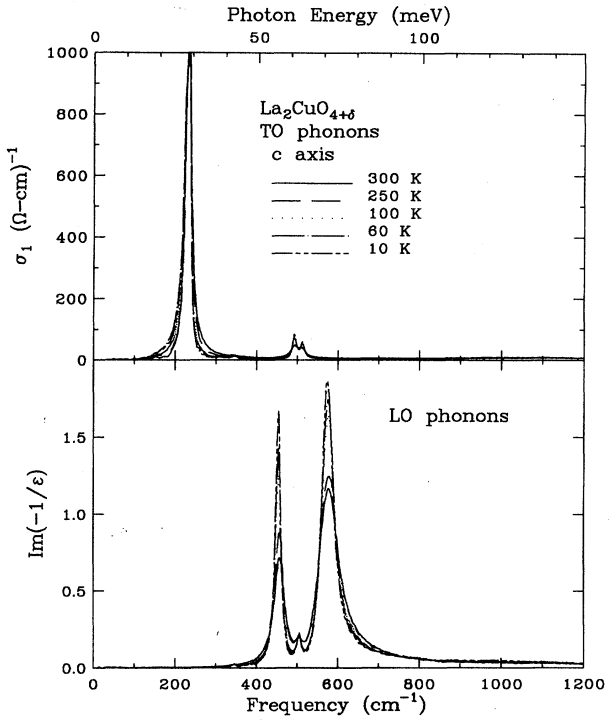

FIG. 5. c-axis optical conductivity (upper panel) and loss function (bottom panel) at several temperatures. The peaks in these quantities give the TO and LO phonon frequencies, respectively.

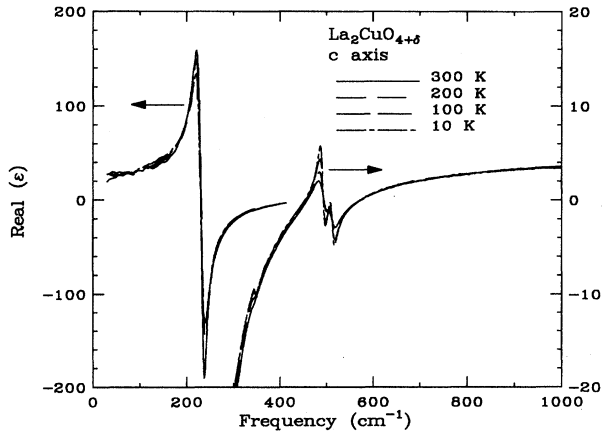

FIG. 6. Real part of the c-axis dielectric function (ϵ_1) at several temperatures.

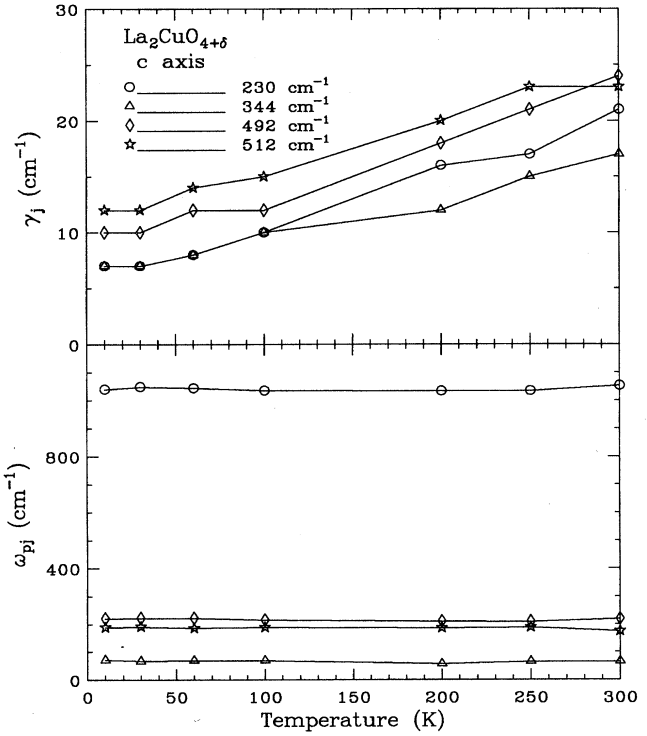

FIG. 7. Temperature dependence of the phonon parameters obtained from Lorentz-model fits to the reflectance: the linewidth γ_j (upper panel) and the oscillator strength ω_{pj} (bottom panel).

atoms into the structure. These additional oxygens, located between adjacent La layers,[20,21] evidently lead to two different force constants between the apical oxygens and the CuO_2 layers.

A quantitative analysis of the intensity and linewidth for each phonon mode as a function of temperature can be done by modeling the reflectance using a dielectric function consisting of four Lorentz oscillators plus a core dielectric constant ϵ_∞ to account for contributions at higher frequencies:

$$\epsilon(\omega)=\sum_{j=1}^{4}\frac{\omega_{pj}^2}{\omega_{jT}^2-\omega^2-i\omega\gamma_j}+\epsilon_\infty, \tag{2}$$

where each term in the sum corresponds to an optical phonon with ω_{pj}, ω_{jT}, and γ_j being the intensity, center frequency, and damping of each mode, respectively. The top panel of Fig. 7 shows the temperature dependence of γ_j, for the jth phonon mode, obtained from a fit to the reflectance at each temperature using Eq. (2). The bottom panel shows the corresponding oscillator strength (ω_{pj}). The results shown in Fig. 7 indicate that most of the temperature dependence in the reflectance is the result of a reduction in γ_j (decrease in the damping) as the temperature of the sample is decreased. There is some saturation in γ_j below 60 K. No anomaly is observed in the superconducting state data. Neither the phonon intensities nor the center frequencies show any significant temperature variation in the measured range; only the mode at 340 cm^{-1} exhibits some slight hardening as the temperature is lowered. The center frequency for this mode increases from 342 cm^{-1} at room temperature to 347 cm^{-1} at $T=10$ K.

TABLE I. Parameters from fits to the room-temperature, c axis reflectance of $La_2CuO_{4+\delta}$. [Note: ω_{jT} and ω_{jL} are the transverse and longitudinal frequencies from Eq. (4) whereas ω_{pj} and γ_j are the oscillator strengths and linewidths from Eq. (2).]

Oscillator	ω_{jT} (cm^{-1})	ω_{jL} (cm^{-1})	ω_{pj} (cm^{-1})	γ_j (cm^{-1})
1	230	342	1052	20
2	342	458	65	15
3	492	507	218	24
4	512	575	174	23
$\epsilon_\infty=5.3$				

C. Oscillator strength and effective charge of the c-axis phonons

The intensities (ω_{pj}) in each phonon line are related to the effective charge that is carried by each ion. In addition, these intensities are also related to the splitting between the transverse optical (TO) and longitudinal optical (LO) phonon frequencies. Since the TO frequencies involve transverse vibrations of the atoms, they are obtained directly from the peak position in the absorption, i.e., the real part of the optical conductivity $\sigma_1(\omega)$. On the other hand, the LO frequencies involve long-range changes in the dipole moment along the direction of phonon propagation in the crystal. Information about the center frequencies of these LO oscillations can be obtained, in principle, from the peak positions in the loss function $-\mathrm{Im}(1/\epsilon)$. An equation which is useful in determining the TO-LO splitting in lattice vibrations is the so-called Lyddane-Sachs-Teller relation. The formula is

$$\omega_{pj}^2=(\omega_{jL}^2-\omega_{jT}^2)\epsilon_\infty. \tag{3}$$

Use of this expression to determine the TO-LO splitting in the present case leads to very poor agreement between the LO frequencies obtained from the peak maxima of the loss function and Eq. (3). The main reason for this is that Eq. (3) is only valid for single or independent oscillators.

We therefore performed a least-square fit to the reflectance data in Fig. 4 using the following factorized expression for $\epsilon(\omega)$. This formula has proven to be appropriate for polar materials such as strontium titanate[46,47]

$$\epsilon(\omega)=\epsilon_\infty\prod_{j=1}^{4}\frac{\omega_{jL}^2-\omega^2+i\gamma_{jL}\omega}{\omega_{jT}^2-\omega^2+i\gamma_{jT}\omega}. \tag{4}$$

The fitting procedure was started by first determining the TO frequencies from the peak maxima of $\sigma_1(\omega)$ and using Eq. (2). Once all the TO frequencies were determined and fixed, the reflectance data were fitted using a program that minimized $\chi^2\sim(R-R_{\mathrm{fit}})^2$ by adjusting the other parameters in Eq. (4). The parameters yielding the best fit to the room-temperature data are displayed in Table I. Although we find good agreement between the LO frequencies obtained from the peak positions of the loss function shown in Fig. 5 and from Eq. (4), assignment of the TO-LO pairs is somewhat

ambiguous. Normally, the TO and LO frequencies should be next to each other with the former having the lower value. In the present case, since the TO mode at 230 cm^{-1} carries most of the spectral weight, the corresponding LO mode is at a much higher frequency than the next TO mode. Hence the ambiguity mentioned above could be attributed to this strong overlapping of the phonon frequencies. This result further invalidates the assumption of independent oscillators implicit in Eq. (3).

As mentioned above, the oscillator strength ω_{pj} of each mode can be used to estimate the effective charge on each ion. An expression that is based on a rigid-ion model of lattice dynamics has been applied successfully to other systems with ionic character.[48] The formula is

$$\sum_j \omega_{pj}^2 = \frac{4\pi}{V} \sum_k \frac{(Z_k e)^2}{m_k}, \tag{5}$$

where V is the volume of the unit cell and the sum on the right-hand side is over all ions with mass m_k and effective charge Z_k. Since the crystal must obey charge neutrality, $\Sigma_k Z_k = 0$. In general, Eq. (5) cannot be solved unless the number of unknown parameters Z_k is less than or equal to 2. In the case of $La_2CuO_{4+\delta}$, since oxygen is much lighter than the other atoms, the right-hand side of Eq. (5) will be dominated, in the first approximation, by the term related to the oxygen atoms. Thus by neglecting all but the oxygen contributions, the result of solving Eq. (5) will yield the effective charge of oxygen averaged over all sites. Such a procedure gives an effective charge for oxygen of $Z_O \sim 1.28$. Similar analyses[1,5] carried out on insulating La_2CuO_4 samples yield an effective charge for oxygen of $Z_O \sim 1.1$. The slightly higher value obtained here is most likely due to the insertion of additional oxygen in the structure. These results differ from the nominal effective charge of two expected for the oxygen in the structure and they indicate the high degree of covalency of the bonds in the structure.

The effects of doping on the 500 cm^{-1} oxygen stretching mode are much stronger than would be expected from the amount of excess oxygen that is in the sample. The mode is split into two modes of approximately equal strength whereas there is only about 3% excess oxygen (or about 6% excess out-of-plane oxygen). The large effects of this relatively small amount of additional oxygen on this mode suggests that the incorporated oxygen introduces a long range distortion of the apical oxygen atom positions, consistent with the observation of superstructure reflections in the electron and neutron diffraction patterns.[20,23,24]

V. *ab*-PLANE SPECTRA

A. Electronic absorption

Figure 8 shows the temperature dependence of the *ab*-plane infrared reflectance measured on face II of the crystal. In the far infrared, we observe an increase in the reflectance with decreasing temperature that is in accord with the increase in the *ab*-plane dc conductivity that is observed in the sample.[27] Evidence of the orthorhombic distortion in the crystal lattice is also clear at low temperatures where weak splittings of the phonon modes at 140 and 680 cm^{-1} are observed.[10] In addition, the weak modes at ~182 and ~296

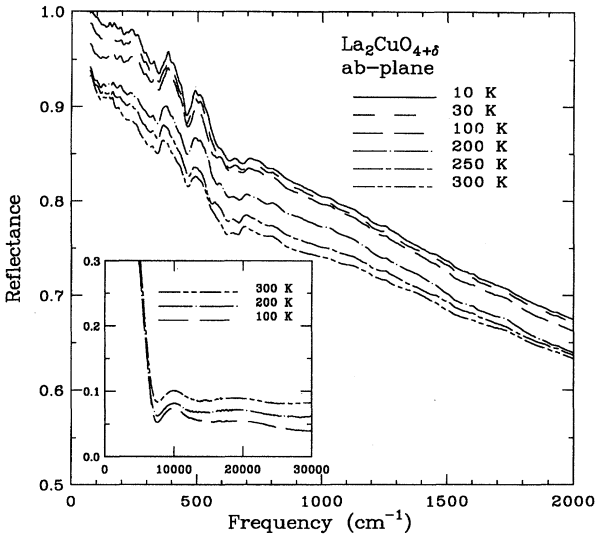

FIG. 8. The *ab*-plane reflectance (face II) of the $La_2CuO_{4+\delta}$ single crystal at temperatures between 10 and 300 K. Inset: The near-infrared and visible *ab*-plane reflectance at three temperatures.

cm^{-1} are more easily resolved at low temperatures. That these infrared-active modes are visible in the spectrum indicates they are incompletely screened by the electronic background.

The inset to Fig. 8 shows the near-infrared and visible reflectance at three selected temperatures. We observe a marked temperature dependence of the reflectance in this range. There is a modest sharpening and steepening of the plasma edge at 7500 cm^{-1} as the temperature of the sample is reduced. At the same time, the reflectance is reduced (sample becomes less reflecting) for frequencies in the visible and above. A similar temperature dependence has been observed in the *ab*-plane reflectance of $La_{2-x}Sr_xCuO_4$ thin films[10] and lightly oxygen-doped $La_2CuO_{4+\delta}$ single crystals.[14] In contrast to the results for Sr-doped films, where a rather abrupt change is observed in the reflectance at 250 K and no change below this temperature,[10] the temperature dependence here is more gradual.

There are two things that can be said about this temperature dependence. In the first place, the fact that there is a broad decrease of the reflectance at lower temperatures implies there should be a temperature dependence to some interband transition at some higher frequency. Secondly, this temperature dependence could be related to oxygen ordering or other structural effects. In $La_{2-x}Sr_xCuO_4$, a tetragonal to orthorhombic transition occurs below room temperature (in samples with the highest T_c). That transition is known to be produced by a small staggered tilt of the apical oxygens in the CuO_6 octahedron. There are two effects associated with this. One of them is a doubling of the basal plane unit cell area in the orthorhombic phase. The second is a redistribution of the electronic density of states near the Fermi surface.[49] According to the measurements of Gao *et al.*,[10] the change in high-frequency reflectance occurs essentially at this transition. We speculate that in $La_2CuO_{4+\delta}$, which already is orthorhombic at room temperature, there is oxygen ordering or growth in the local orthorhombic order occurring

over the broad range between 100 and 300 K, where the high-frequency reflectance is temperature dependent.

B. Assignment of the *ab*-plane phonons

In view of the fact that the crystal structure of La_2CuO_4 is almost tetragonal, with only a weak orthorhombic distortion occurring below 530 K, all phonon lines can be classified under the D_{4h}^{17} point group symmetry. Therefore, the irreducible representation of the vibrations that involve in-plane atomic displacements will correspond to the E_u symmetry. Hence, we expect four infrared-active modes in the in-plane spectrum. Previous studies of the *ab*-plane phonon modes of La_2CuO_4 have identified three E_u symmetry infrared-active modes, at ~140, ~360, and ~690 cm^{-1} in the infrared spectrum.[1-5,7,44,50]

In our oxygen-doped sample, we observe a total of six phonon features, at 80, 140, 230, 355, 484, and 680 cm^{-1}. The greater number of phonon lines in the present sample implies that the assumption of tetragonal symmetry is good only as a first approximation. Nevertheless, the close correspondence of three resonant frequencies in our sample with those of La_2CuO_4 allows us to conclude that they indeed correspond to the E_u symmetry. The low-frequency mode at 140 cm^{-1} corresponds to bending vibrations of the out-of-plane atoms (apex oxygens) against the CuO_2 planes.[5] The remaining two modes, at 355 and 680 cm^{-1}, are related to bending and stretching vibrations respectively of the in-plane Cu-O bonds.

This leaves us with the assignment of the three remaining modes. Raman measurements consistently show Raman-active modes at 230 and 445 cm^{-1} in the undoped material[44,51-55] as well as in samples with excess oxygen.[54] Moreover, a mode at ~90 cm^{-1} has been seen in Sr-doped samples using inelastic neutron scattering[56] and Raman[53] measurements. Based on a tetragonal structure for the unit cell, group theoretical calculations[44,45] indicate that the mode at 230 cm^{-1} is doubly degenerate, with even vibrations having E_g and A_{1g} symmetries. On the other hand, the mode at ~445 cm^{-1} has the A_{1g} irreducible representation. The mode at ~90 cm^{-1} is regarded as belonging to the E_g symmetry.[2,44] Hence, if a correlation is made between the additional infrared modes in this oxygen-doped sample and the Raman-active modes in undoped samples, it can be argued that doping in the material lowers the crystal symmetry making even (gerade) vibrations in the unit cell become infrared active.

There are a number of explanations for an observation of Raman modes in the infrared spectrum. First, if the proposal of *Cmca* space-group symmetry[21] is correct, then the absence of a center of inversion would make these zone-center modes IR allowed as well as Raman allowed. However, if this explanation were adapted, one would also have to understand why these modes are *absent* in La_2CuO_4. Second, disorder, brought on by partial occupancy of the sites where the excess oxygen atoms reside, could also activate Raman modes. However, if there is partial (or total) oxygen ordering as temperature is reduced, as discussed in the Introduction, then the strength of these disorder-induced vibrations would decrease, an expectation contradicted by our data. A third explanation could be that the A_{1g} mode couples to electronic excited states of E_u symmetry making the former infrared

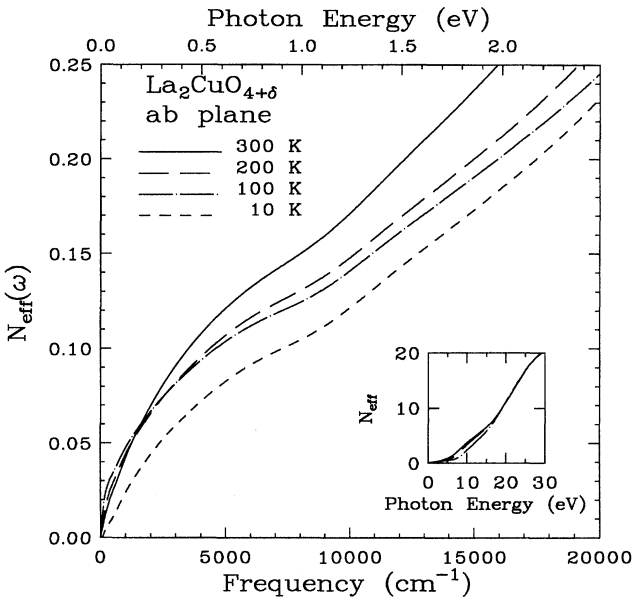

FIG. 9. The partial sum rule spectrum, $N_{eff}(\omega)$, for the *ab* plane at temperatures between 10 and 300 K. The data are per formula unit in $La_2CuO_{4+\delta}$. Inset: Partial sum rule over a wide frequency range, illustrating transfer of oscillator strength from low to high frequencies.

allowed modes. Similar observations have been made by Shimada *et al.*[7] where modes at ~87, ~230, and ~460 cm^{-1} have been observed to grow with Sr doping in $La_{2-x}Sr_xCuO_4$ samples. A final explanation—but only for the mode at 484 cm^{-1}—would assign it as a Fano resonance associated with interactions of the electronic background with the *c*-axis LO phonon modes in the sample. This effect is discussed in Sec. VII, below.

C. Oscillator strength sum rule

Considerable information about the electronic structure can be obtained from a partial sum rule on the optical conductivity. This quantity is defined by

$$N_{eff}(\omega)=\frac{m^* V_{cell}}{4\pi e^2 N_f}\int_0^{\omega}\sigma_1(\omega')d\omega', \tag{6}$$

where m^* is the electron effective mass, V_{cell} is the unit cell volume, N_f is the number of $La_2CuO_{4+\delta}$ formula units per unit cell, and $\sigma_1(\omega)$ is the optical conductivity. It represents the effective number of free electrons participating in optical transitions at frequencies less than ω. Measurements on $La_{2-x}Sr_xCuO_4$ suggest that, in optimally doped samples, $N_{eff}(\omega)$ is nearly equal to the doping level p at frequencies just below the charge-transfer band onset.[8,10]

The result of evaluation of Eq. (6) in our sample is shown in Fig. 9. At each temperature, $N_{eff}(\omega)$ at first rises steeply, begins to level off near 1 eV, and then rises again above the onset of the charge-transfer band. From the behavior below 1 eV, we would estimate that $p\approx 0.15$ in our sample if the average effective mass is the free-electron value.

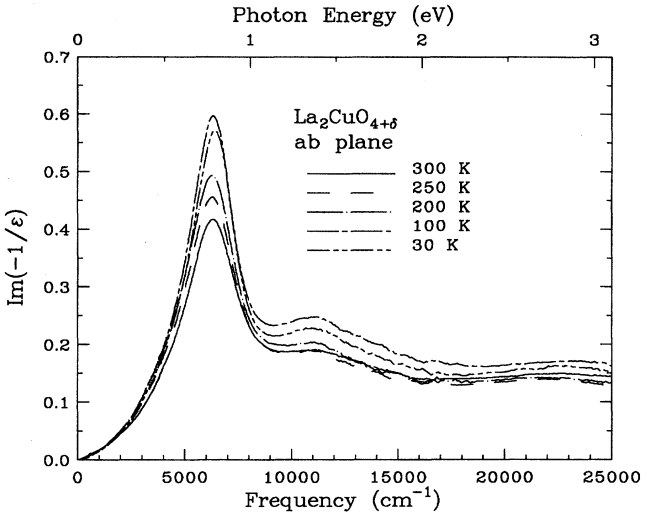

FIG. 10. The loss function, $-\mathrm{Im}[1/\epsilon(\omega)]$, for the ab plane at temperatures between 10 and 300 K.

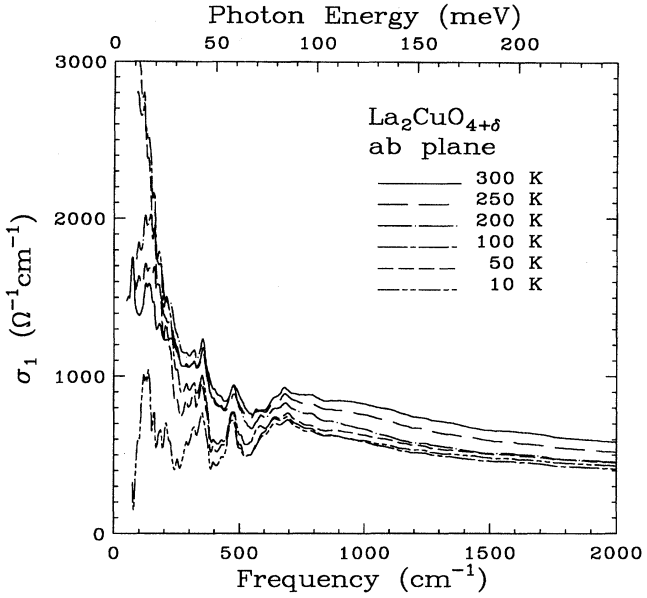

FIG. 11. The far- and midinfrared optical conductivity, $\sigma_1(\omega)$, for the ab plane at temperatures between 10 and 300 K.

There is some variation in N_{eff} with temperature. The variation is largest between 300 and 200 K and again through the superconducting transition. The high-temperature behavior is associated with the changes in near-infrared/visible reflectance seen in Fig. 8 whereas the low-temperature reduction is associated with the appearance of the superconducting condensate. We discuss the former now and will discuss the latter in Sec. VIII.

As mentioned above, we used in our Kramers-Kronig analysis the published results for Sr-doped samples by Tajima *et al.*,[36] which extend up to 40 eV, and a power law, $R\sim\omega^{-4}$, above this energy. It is important in such extensions not to introduce a step in the reflectance where the literature data connect to the experimental reflectance. Such a step would yield false structure in the optical constants. Because there is a temperature dependence in the reflectance all the way up to 38 000 cm^{-1}, the scaling factor used in appending the room-temperature data from Tajima *et al.* to our low-temperature results was reduced in the range 10–15 eV and then joined smoothly to the unchanged data above 15 eV. This procedure made the partial sum rule function, $N_{\mathrm{eff}}(\omega)$, temperature independent above 15 eV. The results for $N_{\mathrm{eff}}(\omega)$ in the high-frequency range are shown in the inset to Fig. 9. They suggest that what occurs in this system as the temperature is reduced is the transfer of some spectral weight from the range where we measured to higher frequencies. This implies a temperature dependence to some interband electronic transition at frequencies higher than 38 000 cm^{-1}. It should be pointed out that doing this extrapolation procedure did not make a significant effect on the results of the Kramers-Kronig analysis below 10 000 cm^{-1} (1.2 eV).

D. Loss function

A second illustration of the high-frequency temperature dependence is shown in Fig. 10. Here, the imaginary part of $-1/\epsilon$ is plotted vs frequency at several temperatures. In ordinary metals, the peak position of this function gives the frequency for plasma excitations of the charge carriers. The width of this peak is related to the lifetime of these excitations. As will be discussed later, the anomalous behavior of the optical conductivity in the high-T_c materials does not allow us to make such an assignment here. A direct consequence of the anomalous absorption in the midinfrared electronic background is the broad width (~0.4 eV) that is observed in the present results and in nearly all copper-oxide superconductors.[8,10,57] The intensity of this peak is larger at low temperatures while the position does not change much as the temperature of the sample is reduced. We also observe a peak at 11 500 cm^{-1} (1.43 eV), which is associated with the charge transfer band in the doped samples. This feature becomes more resolved and shifts slightly towards lower energies at lower temperatures.

Estimates for the screened plasma frequency $\widetilde{\omega_p} \approx \omega_p/\sqrt{\epsilon_\infty}$, can also be deduced from the position of this peak. In the present sample $\widetilde{\omega_p}\simeq 6300$ cm^{-1}. This frequency is nearly the same as in Sr-doped samples.[8,10] In simple metals, the plasma frequency is related to the carrier density p through $\omega_p=\sqrt{4\pi pe^2/m^*}$. However, the cuprates are not simple metals, and a number of experiments have shown that the peak in the loss function (or the plasma minimum in the reflectance) is a very weak function of carrier density.[8,58] Estimates of carrier density should be made from $N_{\mathrm{eff}}(\omega)$ instead of $\tilde{\omega}_p$.

E. ab-plane optical conductivity

The results for the temperature dependence of the ab-plane infrared conductivity $\sigma_1(\omega)$ are shown in Fig. 11. These results were obtained from face II of the crystal. As mentioned before, any structure that may be present in the reflectance is more easily resolved in the spectrum of $\sigma_1(\omega)$. We observe that, as the temperature of the sample is lowered, the phonon modes become sharper. There are also minima or

"notchlike" structures in the frequency range 450–500 cm^{-1} whose possible origin will be discussed later. Moreover, the far-infrared conductivity has a strong temperature dependence, with an increased low-frequency conductivity as the sample is cooled, in accord with the dc transport properties.

The conductivity has a rather weak temperature dependence at midinfrared frequencies. The midinfrared conductivity is reduced when cooling the sample from room temperature to 200 K but there is no appreciable change below this temperature. This behavior is connected with the temperature dependence of the reflectance in the near infrared and visible that is observed in the inset of Fig. 8. As mentioned earlier, a possible explanation could be the growth of local orthorhombic distortions or increased oxygen ordering as temperature is reduced. Similar results at the tetragonal to orthorhombic transition of $La_{2-x}Sr_xCuO_4$ (which occurs in the temperature range 250–300 K) have been reported.[10] In Ref. 10 no further temperature dependence was found above 300 K. A similar experiment was not done in the present sample on account of concern for oxygen loss at temperatures above 300 K.

The conductivity at all temperatures shows a local maximum around 700 cm^{-1}. This maximum becomes more clearly separated from the temperature-dependent part at low frequencies as the temperature is lowered and the latter feature narrows. Above this maximum and up to the onset of the charge-transfer band, the conductivity decreases smoothly.

VI. ANALYSIS OF THE OPTICAL CONDUCTIVITY

A. Dielectric function models

The normal-state $\sigma_1(\omega)$ in Fig. 11 has a frequency dependence that decays much more slowly than the ω^{-2} expected for a material having a simple free-carrier response. This non-Drude behavior, which is universal in the optical conductivity of the copper-oxide superconductors, has been the subject of considerable discussion and controversy.[59–61] The issue is important because the optical conductivity is a direct probe of the electronic structure of the material. The analysis of the optical conductivity has been carried out following several different approaches. In one of those approaches, called the two-component model, the unusual behavior of $\sigma_1(\omega)$ is ascribed to the combination of a free-carrier (Drude) absorption peaked at $\omega=0$ and a broad, bound-carrier absorption centered at higher frequencies.[8,42,62–64] In this picture, the free carriers provide the temperature dependence of the dc resistivity above T_c and condense to form the superfluid below T_c. In contrast the "midinfrared" or bound carriers have a broad frequency response and exhibit very little temperature dependence. There is considerable motivation for this approach: various theories based on Hubbard models, the t-J model, and polarons and bipolarons all predict considerable spectral weight in finite frequency excitons of one sort or another.[65–69]

A second approach is to interpret the anomalous response in $\sigma_1(\omega)$ as the result of a single component of strongly interacting quasiparticles. In this picture, the charge carriers have a frequency- and temperature-dependent self-energy resulting from interactions with some spectrum of excitations. In ordinary metals, this interaction is with the phonons, and leads to Holstein structure in the optical conductivity.[70–72] Although the Holstein effect has been suggested for the non-Drude part of the optical conductivity of the cuprates,[73] the energy scale for the phonons is too low and the coupling too weak to account for the observed spectrum.[10] Thus attention has focussed on non-Fermi-liquid behavior, with strong interactions to a broad spectrum of charge-density and spin-density excitations.[74–76] Models that provide a phenomenological justification for this one-component approach include the "marginal Fermi liquid" (MFL) theory of Varma *et al.*,[77,78] the "nested Fermi liquid" (NFL) theory of Virosztek and Ruvalds,[79,80] and the "Luttinger liquid" picture of Anderson and co-workers.[81]

A third approach is to consider the infrared conductivity as governed by some other physics. Examples of this include the proposal that the conductivity is a paraconductivity involving phase separation, advocated by Emery and Kivelson,[82] and the nearly antiferromagnetic Fermi liquid picture of Monthoux and Pines.[83]

These approaches are discussed in this section. There is one difficulty in comparing the theories with our data. As seen in Fig. 11, there is a resolved peak at ~700 cm^{-1} in $\sigma_1(\omega)$ at all temperatures, suggesting the presence of two or more components to the conductivity. We have therefore performed the analysis of $\sigma_1(\omega)$ based on a decomposition of the conductivity into two parts, a low-frequency part, which is either Drude or non-Drude, depending on the model employed, and a higher-frequency midinfrared contribution. Details of these analyses are presented in the following sections.

B. Two-component picture

The two-component picture is a simple phenomenological scheme for dividing the doping-induced optical conductivity into a free-carrier part and a bound-carrier part. The free carriers are assumed to account for the dc conductivity and far-infrared, T-dependent part of the spectrum while the midinfrared part accounts for the non-Drude part. For the dielectric function, $\epsilon(\omega)$, we use a sum of Drude and Lorentz terms. The Drude model is a reasonable one for the response of free carriers with frequency-independent scattering. However, the Lorentz model is the dielectric function for a harmonic oscillator and the bound-carrier response probably differs considerably from that of a harmonic oscillator. Nevertheless, we use it because it gives a simple closed-form expression for $\epsilon(\omega)$ and represents reasonably the oscillator strength of the midinfrared absorption. We do not take too seriously the central frequency of the linewidths of the oscillators used in the model. The dielectric function is

$$\epsilon(\omega)=-\frac{\omega_{pD}^2}{\omega^2+i\omega/\tau}+\sum_{j=1}^{N}\frac{\omega_{pj}^2}{\omega_j^2-\omega^2-i\omega\gamma_j}+\epsilon_\infty . \quad (7)$$

The first term in Eq. (7) represents the Drude component, described by a plasma frequency ω_{pD} and scattering rate $1/\tau$. The second term is a sum of midinfrared and interband oscillators with ω_j, ω_{pj}, and γ_j being the resonant frequency, oscillator strength, and the width of the jth Lorentz oscillator, respectively. The last term, ϵ_∞, is the high-frequency limit of $\epsilon(\omega)$, and includes interband transitions at frequencies higher than we measure.

A self-consistent approach to separate the Drude-like from the midinfrared contributions has been described by

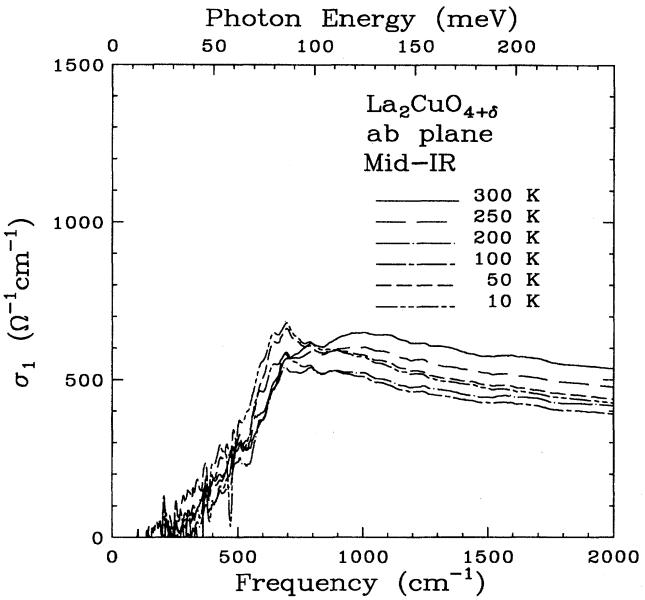

FIG. 12. The ab-plane midinfrared conductivity at several temperatures, obtained by subtracting the Drude contribution and the phonons from $\sigma_1(\omega)$.

Romero *et al.*[84] The basic assumption in this method is that in the superconducting state and for $T \ll T_c$, all the free-carrier part has collapsed into a delta function at $\omega=0$. In first approximation the total conductivity at the lowest temperature would have a negligible free-carrier contribution and will therefore correspond to the midinfrared or bound-carrier component $\sigma_{1\mathrm{MIR}}$ of the total conductivity $\sigma_1(\omega)$. We obtain our first estimate of the free-carrier part in the normal state by subtracting $\sigma_{1\mathrm{MIR}}$ from the experimental $\sigma_1(\omega)$ at $T>T_c$. This first iteration produces free-carrier conductivity ($\sigma_{1D}^{(1)}$) at individual temperatures above T_c. If this conductivity has a Drude line shape, a linear fit to the curve obtained by plotting $1/\sigma_{1D}^{(1)}$ vs ω^{-2} will yield a slope and intercept that can be used to get initial values for ω_{pD} and $1/\tau$. Once values for ω_{pD} and $1/\tau$ are obtained, they can be used to calculate a Drude conductivity from

$$\sigma_{1D}^{\mathrm{fit}}=\frac{1}{4\pi}\frac{\omega_{pD}^2\tau}{1+\omega^2\tau^2}. \tag{8}$$

Then, a new midinfrared conductivity $\sigma_{1\mathrm{MIR}}$ is generated at each temperature by subtracting $\sigma_{1D}^{\mathrm{fit}}$ from the total $\sigma_1(\omega)$ at each temperature above T_c. A self-consistent check of the ω_{pD} and $1/\tau$ obtained at each temperature is done by first computing an average midinfrared conductivity $\langle\sigma_{1\mathrm{MIR}}\rangle$ from the $\sigma_{1\mathrm{MIR}}$ obtained as explained above, and using this average as the starting midinfrared term in a second iteration. We found the method converges after a few (3 or 4) iterations.

The midinfrared conductivity is shown in Fig. 12. This shows the conductivity with the conductivity from the ab-plane phonons and the free carriers subtracted. The midinfrared part shows some interesting features. The overall oscillator strength of the midinfrared conductivity appears to decrease as the temperature of the sample is decreased from room temperature down to 200 K. A less noticeable change is seen below this temperature. This temperature dependence is connected to the decrease that is seen in the near-infrared reflectance shown in the inset of Fig. 8. As discussed already, it appears that some spectral weight is being transferred to higher frequencies, affecting $\sigma_1(\omega)$ in the midinfrared. In contrast the oscillator strength of the Drude part, responsible for the dc conductivity in the two-component model, does not change with temperature. We also observe a bumplike structure, which at 300 K appears at around 1000 cm^{-1}, and which diminishes in intensity with a reduction in temperature. Then, at about 200 K, a second and sharper feature appears at a lower energy, ~750 cm^{-1}, growing in intensity as the temperature of the sample is further reduced. Similar midinfraredlike modes in the optical conductivity of both lightly doped[14,85] and superconducting samples have been reported in the literature.[10,42,86,87] The present results underscore the generality of these features in the optical properties of the copper-oxide-based materials.

The Drude component in this analysis carries about 22% of the total doping-induced spectral weight. There are two constraints that this component should satisfy if the two-component picture is to be a reasonable approach to optical properties. First, the spectral weight of the Drude component should be (approximately) independent of the temperature, as expected for metallic charge carriers. (In principle, one can allow for thermal expansion and for changes in electronic structure brought on by effects as oxygen ordering or antiferromagnetism.) Second, the temperature dependence of the scattering rate should imply relatively weak coupling to the excitations responsible for the scattering so that Holstein structure[70–72] is absent from the free-carrier conductivity. (A third constraint, that $1/\tau$ be linear in temperature, is implied already by the constancy of ω_p and the good agreement between optical conductivity and dc conductivity temperature dependence.)

The two-component analysis is in accord with these expectations. The Drude plasma frequency has a magnitude of $\omega_{pD}\sim 5660\pm 100$ cm^{-1} for all temperatures between 30 and 300 K. The scattering rate of the free-carrier or Drude contribution has a linear temperature dependence, shown in Fig. 13, as expected from the dc resistivity. The linear $1/\tau$ is of course one of the hallmarks of the cuprate superconductors. In ordinary metals, $1/\tau$ linear in temperature is the high-temperature limit of scattering from some excitations like the phonons. In that case, $1/\tau=2\pi\lambda T+1/\tau_0$, where λ is the strength of the electron-phonon coupling constant. If we use this formula for our data, the straight line fit, shown in the figure, yields a value for the coupling constant $\lambda\simeq 0.25$. This is indeed a weak coupling value and agrees with what has been found by similar analyses in other materials.[10,42,84]

We were not able to measure the dc resistivity of the actual sample studied by far-infrared measurements. When the far-infrared results are compared to the dc resistivity measurements of a similar sample,[27] there is a disagreement in magnitude but agreement in the temperature dependence. The dc and far-infrared conductivities differ by about a factor of 4; at 300 K $\rho_{\mathrm{dc}}\simeq 2.5$ mΩ cm whereas $\rho_{\mathrm{FIR}}\simeq 0.6$ mΩ cm. Both dc and far infrared show a quasilinear decrease in resistivity with decreasing temperature, with a nonzero intercept in a linear extrapolation to $T=0$. We do not know if the discrepancy is one of differing samples or systematic mea-

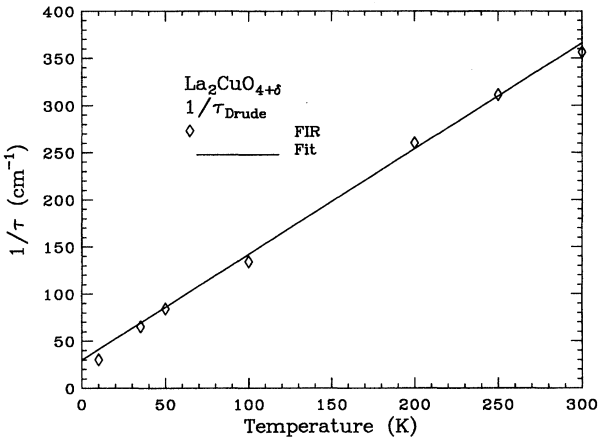

FIG. 13. The scattering rate of the Drude contribution from a two-component fit to the optical conductivity shown in Fig. 11. (Notice the linear temperature dependence.)

surement errors. Typically, the agreement between dc and far-infrared measures of resistivity is rather good.[10,42,64]

The left panel of Fig. 14 illustrates the two-component fit. The optical conductivity at 50 and 200 K, with the phonons subtracted, is plotted along with the best fit from this model. The dashed lines show the individual components of the fit to the 50 K data. The Drude part (long dashes) dominates below 400 cm^{-1}; above this frequency a broad midinfrared oscillator dominates. A narrow oscillator accounts for the sharp feature at 750 cm^{-1}. The low-frequency wings of a third oscillator, that is centered at 3800 cm^{-1}, may also be seen.

C. Generalized drude approach

In models such as the MFL or NFL, the imaginary part of the quasiparticle self-energy is written as[77–80]

$$-\mathrm{Im}\,\Sigma(\omega)\sim\begin{cases}\pi^2\lambda T, & \omega<T\\ \pi\lambda\omega, & \omega>T,\end{cases} \tag{9}$$

where λ is a dimensionless coupling constant and T is the temperature. Hence, for $\omega<T$, it is seen that $-\mathrm{Im}\Sigma$ is linear in temperature, which is consistent with fact that the resistivity has a linear temperature dependence in nearly all copper-oxide superconductors. As ω increases, reaching a magnitude of order of T or higher, a new spectrum of excitations arises. This causes $-\mathrm{Im}\Sigma$ to grow linearly with frequency up to a cutoff frequency ω_c.

The dielectric function can be written as[88]

$$\epsilon(\omega)=\epsilon_\infty-\frac{\omega_p^2}{\omega[\omega-2\Sigma(\omega/2)]}, \tag{10}$$

where the factors of 2 arise because quasiparticle excitations come in pairs, ϵ_∞ is a constant that includes contributions from interband transitions, and ω_p is the bare plasma frequency for the charge carriers, defined by $\omega_p^2=4\pi ne^2/m_b$ with n the carrier density and m_b the band mass of the carriers. The quantity $\Sigma(\omega)$ represents the quasiparticle self-energy. The real part of Σ is related to the effective mass m^* of the interacting carriers by[78] $m^*(\omega)/m_b=1-2\,\mathrm{Re}\,\Sigma(\omega/2)/\omega$ whereas the imaginary part is related to the quasiparticle lifetime through $1/\tau^*(\omega)=-2m_b\,\mathrm{Im}\,\Sigma(\omega/2)/m^*(\omega)$.

A number of authors have analyzed optical data for $La_{2-x}Sr_xCuO_4$ using such a one-component approach, obtaining either $-\mathrm{Im}\,\Sigma$ or (nearly the same thing) $1/\tau$ to be almost linear in frequency.[10,89] However, in other cases, no such linear dependence can be found.[7,8] Our data fall into this second category. In fact, because there is a rather well-defined peak at ~700 cm^{-1} in the optical conductivity of Fig. 11, it is not appropriate to invert the dielectric function to obtain the scattering rate or self-energy, as has been done for $YBa_2Cu_3O_{7-\delta}$ (Refs. 75, 90) and $Bi_2Sr_2CaCu_2O_8$.[86] Instead, it seems necessary to allow for a second component in

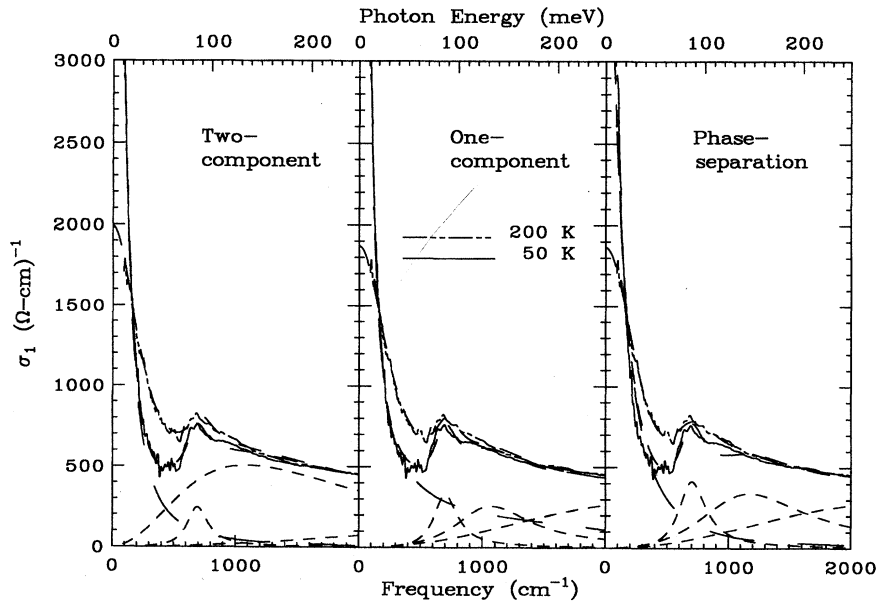

FIG. 14. The *ab*-plane optical conductivity (with phonon contribution subtracted) at 50 and 200 K compared to model calculations. The various terms in the fits to the 50 K data are also shown: the term responsible for the dc conductivity with long dashed lines and the Lorentz oscillators with short dashed lines. Left panel: Two component fit. Center panel: One-component fit. Right panel: Fit to model based on phase separation.

addition to the generalized Drude one. Thus we have performed a least-squares fit to a model given by

$$\epsilon(\omega)=-\frac{\omega_p^2}{\omega[\omega-2\Sigma(\omega/2)]}+\sum_{j=1}^{N}\frac{\omega_{pj}^2}{\omega_j^2-\omega^2-i\omega\gamma_j}+\epsilon_\infty . \tag{11}$$

The first term in Eq. (11) is the MFL or NFL component; the second term is a sum of oscillators to represent some additional midinfrared band; ϵ_∞ describes the charge-transfer and higher-frequency interband transitions.

The center panel of Fig. 14 illustrates the one-component fit. The optical conductivity at 50 and 200 K, with the phonons subtracted, is plotted along with the best fit from this model. The dashed lines show the components of the fit to the 50 K data. The MFL or NFL part (long dashes) dominates below about 1000 cm^{-1}; above this frequency three midinfrared oscillators dominate. A narrow oscillator accounts for the sharp feature at 750 cm^{-1}. The oscillator at 1000 cm^{-1} is considerably weaker than in the two-component fit while the third oscillator, centered at 3800 cm^{-1} (whose low-frequency wing may be seen in the figure) is stronger than in the two-component fit. The introduction of a frequency-dependent relaxation rate extends the tail of the free-carrier component to higher frequencies. However, less than half of the doping-induced oscillator strength is associated with the mobile carriers. Indeed, most of the oscillator strength above 700 cm^{-1} is associated with the bound-carrier components.

The fit is more than acceptable. However, in order to obtain a reasonable fit, we had to allow the coupling constant λ to be temperature dependent. At 50 K we get $\lambda=0.10$ while at 200 K $\lambda=0.20$. A similar result was found for $La_{2-x}Sr_xCuO_4$ films by Gao *et al.*[10] This temperature dependence is not included in the usual models that lead to the one-component picture.

D. Phase-separation model

Emery and Kivelson[82] have discussed evidence that the carriers in cuprates are susceptible to phase separation. This tendency is driven by the lower energy of a tightly-bound spin singlet but frustrated by the long-range Coulomb interaction. A result of their model is a characteristic frequency and temperature dependence to the optical conductivity:[91]

$$\sigma_1(\omega)=e^2A\,\frac{\chi_2(\omega,T)}{\omega}+(e^\star)^2\omega\chi_2(\omega,T). \tag{12}$$

The two terms in Eq. (12) represent respectively the motion of free carriers and the direct response of local "dipolar" modes. The latter arise from density fluctuations caused by the desire for phase separation. The other quantities are e and $e^\star$, the charges of the mobile carriers and dipolar fluctuations, respectively, $A=(2a\Delta J_\parallel/\pi)^2$ with a the lattice constant and $\Delta J_\parallel$ describing the coupling between the electron gas and the dynamical scattering centers.[91] The quantity $\chi_2(\omega,T)$ is a susceptibility, given by

$$\chi_2=c\,\tanh(\omega/2T)\,\frac{\Gamma}{\Gamma^2+\omega^2},$$

with c the concentration of dipolar centers and Γ the Kondo scale of the problem, here taken of order $J\approx1000$ K. At low frequencies, the conductivity of Eq. (12) is dominated by the first term and gives $\sigma_1(0)\propto1/T$ whereas at high frequencies the second, or bound-carrier, part dominates and $\sigma_1(\omega)$ is T independent.

The right panel of Fig. 14 illustrates a fit to this phase-separation model. As in the previous case, a good fit could not be obtained without also including additional midinfrared oscillators. The optical conductivity at 50 and 200 K, with the phonons subtracted, is plotted along with the best fit from the model. The dashed lines show the components of the fit to the 50 K data. In order to obtain a physically reasonable fit, we constrained the oscillator strength of the conductivity in Eq. (12) to be the same at all temperatures, equal to what the fit found at the lowest temperature, and fixed the parameter $\Gamma=500$ cm^{-1}. (Otherwise, the fit drove it to zero.) The conductivity from Eq. (12) dominates below about 500 cm^{-1}; above this frequency three midinfrared oscillators dominate. A narrow oscillator accounts for the sharp feature at 750 cm^{-1}. The oscillator at 1000 cm^{-1} is somewhat weaker than in the two-component fit while the third oscillator, centered at 3800 cm^{-1}, is stronger. The introduction of a frequency-dependent relaxation rate extends the tail of the free-carrier component to higher frequencies. About 30% of the doping-induced oscillator strength is associated with the combined terms in Eq. (12).

This model can describe the optical conductivity only if there are additional midinfrared contributions. In addition, the value of Γ that gives an acceptable fit, 500 cm^{-1}, is lower than one would like if Γ is to be of order J, which is typically more like 1000 cm^{-1}. Finally, we note that the quantity A had to be changed by about 20% between 50 and 200 K in order to have a good fit.

E. Other approaches to the *ab*-plane optical conductivity

We have not calculated the conductivity within the nearly antiferromagnetic Fermi liquid picture of Monthoux and Pines.[83] However, judging from the fits to $YBa_2Cu_3O_{7-\delta}$ in Ref. 83, we expect that the results would be similar to the other cases we have considered: the model can fit the data below about 0.1 eV but does not describe the conductivity above this frequency.

As mentioned above, there are a number of numerical calculations of the optical conductivity which give a midinfrared absorption due to finite frequency excitons of one sort or another.[65–69] Generally speaking, these provide spectral weight in about the right energy range and of about the right amount and so may be said to be in accord with our measurements.

Another proposal for midinfrared absorption, put forward by Bi and Eklund,[92] attributes it to photon-assisted hopping of small polarons. Bi and Eklund were able to fit room-temperature data for $La_{2-x}Sr_xCuO_4$, $La_{2-x}Sr_xNiO_{4+\delta}$, and other materials within such a model. We find that we cannot reconcile our data with this model, because it predicts a strong temperature dependence to the optical conductivity. (For example, the model predicts that the spectral weight will change by a factor of 2 between 200 and 300 K.) Our data are—to first approximation—temperature independent.

VII. COMPARISON OF *ab*-PLANE REFLECTANCE: $\mathbf{q}\|c$ AND $\mathbf{q}\perp c$

One recent issue in the study of the infrared properties of the copper-oxide superconductors is the effect of the electron-phonon interaction. Early on, evidence for the importance of this interaction had been gathered mainly from neutron time-of-flight spectroscopy, where a softening of the phonon density of states was observed when the doping level in $YBa_2Cu_3O_{6+x}$ was changed from the insulating to the metallic regime.[93] There was also evidence for anomalies in certain phonon branches associated with stretching modes of Cu-O bonds near the zone boundary.[94] Such interactions might be invoked to explain the linearity of the normal-state resistivity as a function of temperature that is observed in nearly all copper-oxide superconductors. This explanation would imply that the charge carriers are scattered by some sort of thermal excitations such as phonons. However, this interpretation should be taken with some caution, because in ordinary metals the T-linear resistivity is a high-temperature phenomenon whereas in the high-T_c materials this T-linear behavior is observed even below the Debye temperature, where a T^5 or T^3 behavior should be expected.

The type of electron-phonon interaction that is considered to be relevant for the optical absorption is the one that occurs in organic conductors.[95] In these materials, as first pointed out by Rice,[96] linear coupling of charge carriers to totally symmetric A_g modes gives structure in the conductivity spectrum at infrared frequencies. The overlapping of these phonon frequencies with the continuum of excitations gives rise to minima or characteristic Fano line shape antiresonances in the conductivity spectrum. It has been proposed[63,97] that similar effects in the copper-oxide superconductors could give rise to the "kneelike" structures that are seen at 140 and 440 cm^{-1} in the ab-plane reflectance spectrum of $YBa_2Cu_3O_{7-\delta}$.[42,64] These structures show up as an onset at lower energy and a "notch" at higher energy in the spectrum of $\sigma_1(\omega)$. Similar features have also been seen in the conductivity spectra of $Bi_2Sr_2CaCu_2O_8$,[86,98] $La_{2-x}Sr_xCuO_4$,[7,10] and $Pb_2Sr_2(Y/Ca)Cu_3O_8$.[87]

A physical origin for this structure has been given by Reedyk *et al.*,[28] who proposed that the coupling in the high-T_c and isostructural materials is between the c-axis LO phonons and the ab-plane bound (or "midinfrared") carriers. This idea is based on the observation that the coupling and, hence, the presence of structure in $\sigma_1(\omega)$ is enhanced in the so-called parallel geometry, i.e., when measurements of the ab-plane optical reflectance are performed when the wave vector of the incident light $\mathbf{q}$ is parallel to the c axis of the sample and the electric field $\mathbf{E}$ is polarized within the ab plane. The structure is weaker when the ab-plane optical properties are measured on the ac (or bc) face of the crystal.[87] In this geometry, the wave vector of the light, which lies either along the a or b axis, is perpendicular to the c axis.

In order to illustrate the effect of electron-phonon coupling in our sample, we display in Fig. 15 the ab-plane reflectance when the wave vector of the light $\mathbf{q}$ is parallel and perpendicular to the c axis in the sample. A comparison of the two room-temperature spectra indeed finds some differences. When $\mathbf{q}\|c$, the far-infrared reflectance displays two

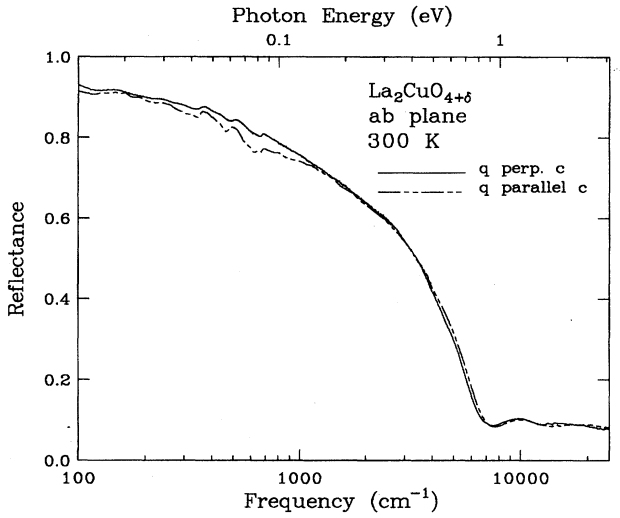

FIG. 15. A comparison of the ab-plane reflectance measured from face I ($\mathbf{q}\perp$c) and face II ($\mathbf{q}\|c$) of $La_2CuO_{4+\delta}$ at $T=300$ K.

shoulders each followed by minima at higher frequencies. Such structures are reduced in the case when $\mathbf{q}\perp c$. A second observation is that at higher frequencies both reflectance spectra are nearly the same with only a slight shift of the plasma edge minima. Also, the charge transfer band, located around 12 000 cm^{-1}, appears to have equal strength in both spectra. Because the strength of this band gives an indication of the doping in the sample, this means that both surfaces of the crystal have nearly equal doping.

To illustrate further the differences at low frequencies, we show in the top part of Fig. 16 the optical conductivity $\sigma_1(\omega)$ obtained from a Kramers-Kronig analysis of the reflectance in the two geometries indicated above. For more clarity, we have subtracted the phonons that are present in both spectra. This figure clearly shows that $\sigma_1(\omega)$ displays two minimalike structures at 450 and 560 cm^{-1}. A remarkable coincidence exists between these frequencies and the peak positions of the c-axis LO phonon frequencies, as determined from the peak maxima of the c-axis loss function $-\mathrm{Im}(1/\epsilon)$ for the same sample. This function is also shown in the figure. Another observation is that there is a redistribution of spectral weight from low to high frequencies in the spectrum when $\mathbf{q}\|c$. The midpoint of such redistribution appears to coincide with the peak position of the strongest c-axis LO phonon at 560 cm^{-1}. This redistribution conserves the sum rule for the two propagation directions, as shown in the bottom part of Fig. 16. These results clearly underscore the importance of electron-phonon coupling in the optical properties of the high-T_c materials.

VIII. SUPERCONDUCTING STATE

One motivation for infrared spectroscopy in the high-temperature superconductors is the search for the superconducting energy gap; in consequence, this issue has been rather controversial over the years.[59–61] We discuss the measurements in the superconducting state in this section. The reason for the controversy can be explained by considering Figs. 11 and 12. Figure 11 shows the optical conductivity at

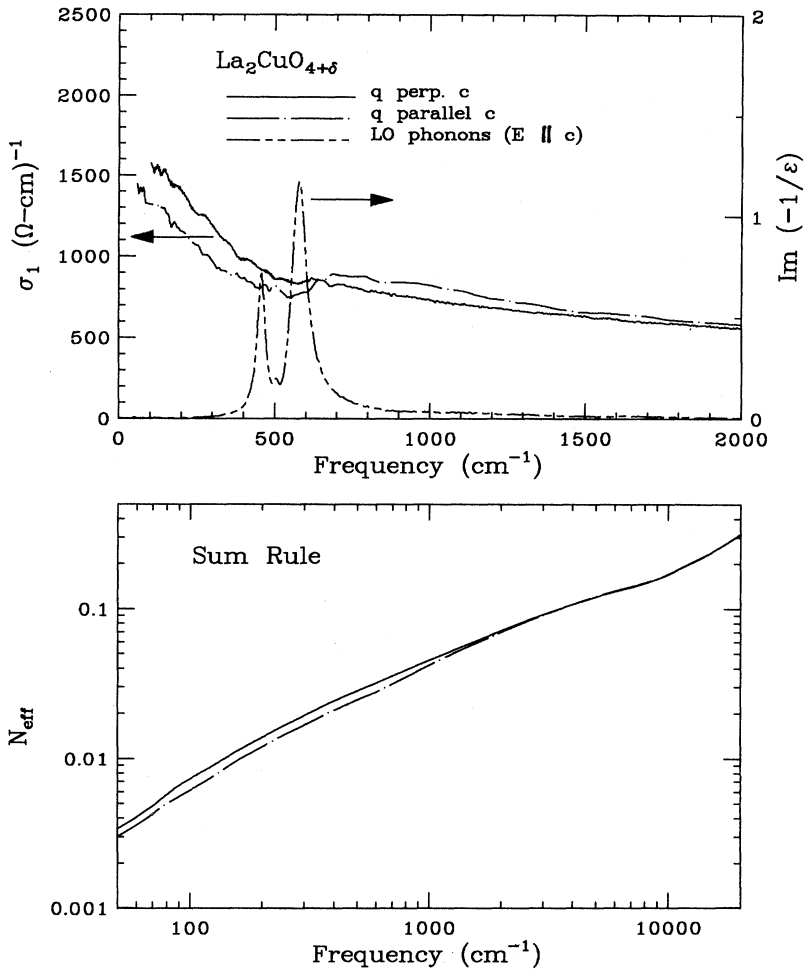

FIG. 16. Top: A comparison of the ab-plane conductivity measured on the sample for $\mathbf{q}\perp c$ (face I) and $\mathbf{q}\|c$ (face II) at $T=300$ K. Bottom: Sum rule of the reflectance at room temperature for $\mathbf{q}\|c$ and $\mathbf{q}\perp c$.

several temperatures above and below T_c. In the 10 K spectrum, the rise in $\sigma_1(\omega)$ as $\omega\rightarrow 0$ which is seen in the normal state spectra is absent. A number of features remain in the spectrum and one may question whether any is related to the gap. Note that the BCS gap for a $T_c=40$ K superconductor would be 100 cm^{-1} whereas $8k_BT_c$ is 220 cm^{-1}, and that there is structure in $\sigma_1(\omega)$(10 K) at these (and other) frequencies. That this structure is probably not the gap can be seen by inspecting Fig. 12, which shows the optical conductivity with a Drude spectrum and the contribution of the ab-plane optical phonons subtracted. In this presentation of the data, it is difficult to see that there are any features in the 10 K measurement that are not in the data above T_c. The same results have been found in $YBa_2Cu_3O_{7-\delta}$ by Kamarás *et al.*[42]

To illustrate this more clearly, we show in Fig. 17 the conductivity at 10 K and at 50 K. The amount of spectral weight that goes into the delta function is evident from these two curves. The third line in Fig. 17 is the midinfrared spectrum at 50 K, obtained by subtracting a Drude curve characterized by a plasma frequency $\omega_{pD}=5700$ cm^{-1} and a width $1/\tau=84$ cm^{-1} (giving a dc conductivity of 6500 Ω^{-1} cm^{-1}). Aside from a somewhat higher level (which we attribute to a residual normal fluid at 10 K) the 10 and 50 K midinfrared spectra are quite similar.

The superconducting-state conductivity has been recently calculated within a d-wave pairing scenario by Hirschfeld.[99] Even at $T=0$ the conductivity has a large low-frequency value on account of the nodal structure in the gap function. There is a deep minimum at $\sim 2\Delta_0$, where Δ_0 is the maximum gap, and a maximum near $\sim 4\Delta_0$. This maximum at $\sim 4\Delta_0$ is a sort of Holstein sideband resulting from a combined process of pair breaking and scattering from a spin fluctuation. Our data are not inconsistent with the main feature of large low-frequency conductivity; however, the predicted structure does not emerge.

There is clearly a condensate in the superconducting state. Its oscillator strength can be estimated in two ways. In the partial sum rule plot of Fig. 9, the 10 K curve is systematically below the 100 K curve. This difference occurs because the numerical integration of Eq. (6) has not included the weight of the delta function in the superconducting conductivity. The number of effective electrons/formula unit making up the condensate, $N^s_{\rm eff}$ is then $N^s_{\rm eff}=0.029$, or about 18% of the total doping-induced oscillator strength. Expressed as a plasma frequency, $\omega_{ps}=(4\pi n_s e^2/m)^{1/2}$, this translates to $\omega_{ps}=5000\pm 100$ cm^{-1}.

The equivalent functions $\epsilon_1(\omega)$, $\sigma_2(\omega)$, and $\lambda_L(\omega)$ give a second estimate of the oscillator strength of the

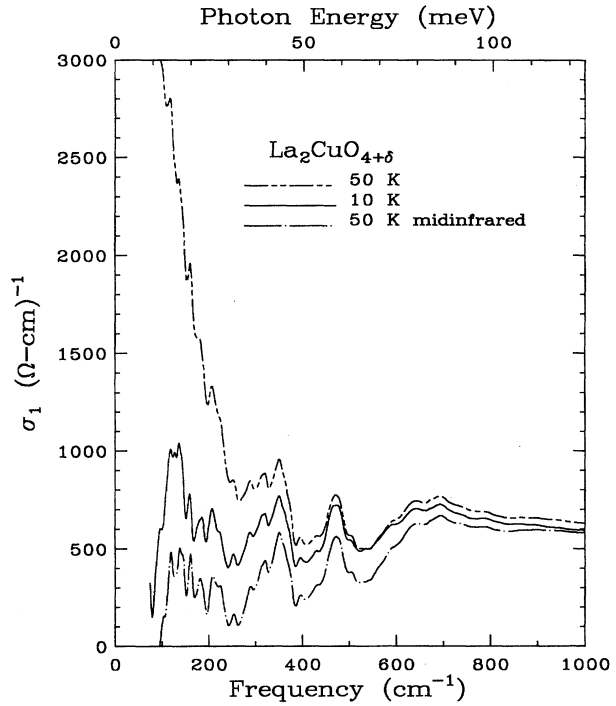

FIG. 17. The ab-plane optical conductivity of $La_2CuO_{4+\delta}$ at 10 and 50 K, along with the 50 K midinfrared conductivity.

condensate.[42,100] Figure 18 shows $\lambda_L(\omega)$, defined as $\lambda_L(\omega) = \sqrt{c/4\pi\sigma_2(\omega)}$ where c is light speed and $\sigma_2(\omega)$ the imaginary part of the optical conductivity. That this function is nearly constant is a consequence of the fact that $\sigma_2(\omega) \gg \sigma_1(\omega)$ at low frequencies. The ab-plane penetration depth is about 3100 Å; expressed as a plasma frequency, this translates to $\omega_{ps} = 5100 \pm 200$ cm^{-1}. This penetration depth is larger (carrier density smaller) than the 2750 Å estimated for a $La_{2-x}Sr_xCuO_4$ film,[10] and also larger than the 2500–3000 Å found by μSR experiments.[101,102]

The two estimates of the superfluid oscillator strength agree. Note that the superfluid density from these arguments

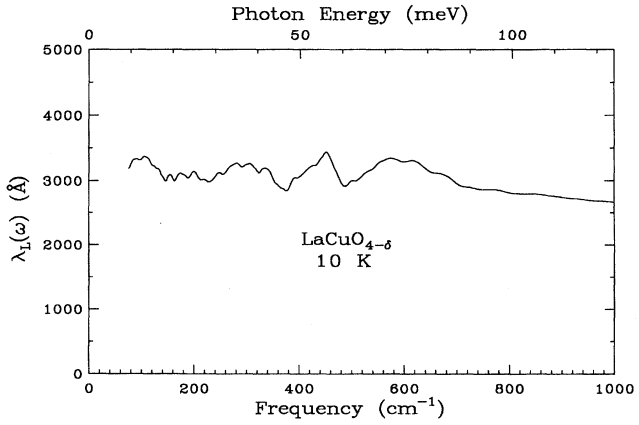

FIG. 18. The ab-plane penetration depth of $La_2CuO_{4+\delta}$ determined by infrared means.

is about 80% of the free-carrier density estimated by the two component fit. In $La_{2-x}Sr_xCuO_4$ Gao *et al.*[10] estimated that about 85% of the free-carrier density went into the condensate. These numbers are consistent with the basic clean-limit argument, that with most of the spectral weight from the free carriers in the condensate response, there is little left for transitions across the gap.[42]

The clean-limit argument depends on the presence of two components to the optical conductivity in the frequency region where the gap exists. If there is only a single component, as in the MFL or NFL, then the 10 K conductivity spectrum must represent the excitations across the gap, at least up until the point ($\sim$500 cm^{-1}) where other excitations begin. A difficulty with this interpretation is that the spectral weight associated with the gap transitions cannot be accounted for within a realistic model for the materials.[103]

IX. CONCLUSIONS

In sum, results for polarized reflectance of superconducting $La_2CuO_{4+\delta}$ ($T_c \simeq 40$ K) reveal an insulator for polarization of the light along the c axis, while the ab-plane response has metallic properties. A total of four optic phonons, one more than in insulating La_2CuO_4, are resolved in the c-axis polarization. The additional mode is interpreted as a splitting of the oxygen stretching mode brought on by the insertion of excess oxygen in the crystal. Using a rigid-ion model, we find an estimate of the average oxygen effective charge in the structure to be 14% higher than in insulating La_2CuO_4.[5] This is close to the estimated 12% oxygen doping in the sample as well as the estimated carrier concentration p.

We have made estimates of p from two measurements: the total spectral weight below the charge transfer gap, which yielded $p \approx 0.15$, and the c-axis plasma frequency in the superconducting state, which yielded $p \approx 0.11$. Two other measures of the carrier concentration are the free-carrier (Drude) plasma frequency and the London penetration depth of the superconducting phase. These are both dependent on p/m^*, but since we do not know m^*, all we can do is compare these numbers to the results of Gao *et al.*[10] for a $La_{1.83}Sr_{0.17}CuO_4$ film and assume that (1) the Sr content equals the carrier density, and (2) m^* is not a strong function of carrier density. Under these assumptions, the free-carrier plasma frequency of 5660 cm^{-1} when compared to the 6300 cm^{-1} found for the Sr doped sample implies $p \approx 0.14$ while the penetration depths (3100 Å here and 2750 Å in the Sr-doped sample) give $p \approx 0.13$. Finally, comparison of our room-temperature conductivity and $N_{\rm eff}(\omega)$ to the results for a series of Sr-doped samples by Uchida *et al.*[8] also suggests p in the 0.13–0.14 range. Thus, because the oxygen content in our sample is believed to be $\delta \approx 0.12$, our results support the work[16,20,25] which indicates that each excess oxygen contributes just over one hole, ($p/\delta \sim 1.1$).

We also find an anomalous temperature dependence in the ab-plane reflectance for frequencies in the visible and above. This result may indicate some restructuring of the electronic interband transitions, possibly due to an increased order in the positions of the excess oxygen atoms at lower temperatures or to a larger orthorhombic distortion at lower temperatures. This transition appears also to affect the oscillator

strength of the midinfrared conductivity. At the same time, it does not appear to affect the oscillator strength of the free-carrier contribution in a two-component analysis of $\sigma_1(\omega)$. In this analysis, we find $\omega_{pD} \sim 5660 \pm 100$ cm^{-1} with a scattering rate that is linear in temperature.

In the superconducting state 80% of this free-carrier oscillator strength appears in the zero-frequency δ-function conductivity of the condensate, giving a penetration depth of 3100 Å. There is no signature of a superconducting gap in our spectrum.

A comparison of the ab-plane optical conductivity obtained from two different faces reveals qualitative differences. In the case when the wave vector of the light is parallel to the c axis, the midinfrared conductivity shows two minima whose positions are correlated with the peaks in the LO frequencies of the c-axis phonons. Such features are nearly absent in the spectrum of $\sigma_1(\omega)$ measured when $\mathbf{q} \perp c$. This, combined with the fact that the coupling constant obtained from the slope of the linear temperature dependence of $1/\tau$ of the Drude-like carriers in a two-component analysis of $\sigma_1(\omega)$ is rather small ($\lambda \simeq 0.25$), suggests that the c-axis LO phonons are more strongly coupled to the midinfrared carriers than to the free carriers.

ACKNOWLEDGMENTS

We thank Elihu Abrahams, Piers Coleman, Vic Emery, Peter Hirschfeld, and Steven Kivelson for stimulating discussions about the optical properties. The work at Florida is supported by National Science Foundation, Solid State Physics Program, Grant No. DMR-9403894. Ames Laboratory is operated for the U.S. Department of Energy by Iowa State University under Contract No. W-7405-ENG-82. The work at Ames was supported by the Director for Energy Research, Office of Basic Energy Sciences.

*Present address: Department of Physics and Astronomy, University of Maryland, College Park, MD 20742.

†Present address: Center for Materials Science and Engineering, Massachusetts Institute of Technology, Cambridge, MA 02139.

[1] F. Gervais, P. Echegut, J. M. Bassat, and P. Odier, Phys. Rev. B **37**, 9364 (1988).

[2] P. C. Eklund, A. M. Rao, G. W. Lehman, G. L. Doll, M. S. Dresselhaus, P. J. Picone, D. R. Gabbe, H. P. Jenssen, and G. Dresselhaus, J. Opt. Soc. Am. B **6**, 389 (1989).

[3] R. T. Collins, Z. Schlesinger, G. V. Chandrashekhar, and M. W. Shafer, Phys. Rev. B **39**, 2251 (1989).

[4] A. V. Bazhenov, T. N. Fursova, V. B. Timofeev, A. S. Cooper, J. P. Remeika, and Z. Fisk, Phys. Rev. B **40**, 4413 (1989).

[5] S. Tajima, T. Ido, S. Ishibashi, T. Itoh, H. Eisaki, Y. Mizuo, H. Takagi, and S. Uchida, Phys. Rev. B **43**, 10 496 (1991).

[6] J. P. Falck, A. Levy, M. A. Kastner, and R. J. Birgeneau, Phys. Rev. Lett. **69**, 1109 (1992).

[7] M. Shimada, M. Shimizu, J. Tanaka, I. Tanaka, and H. Kojima, Physica C **193**, 277 (1992).

[8] S. Uchida, T. Ido, H. Takagi, T. Arima, Y. Tokura, and S. Tajima, Phys. Rev. B **43**, 7942 (1991).

[9] K. Tamasaku, Y. Nakamura, and S. Uchida, Phys. Rev. Lett. **69**, 1455 (1993).

[10] F. Gao, D. B. Romero, D. B. Tanner, J. Talvacchio, and M. G. Forrester, Phys. Rev. B **47**, 1036 (1993).

[11] D. A. Bonn, J. E. Greedan, C. V. Stager, T. Timusk, M. G. Doss, S. L. Herr, K. Kamarás, C. D. Porter, D. B. Tanner, J. M. Tarascon, W. R. McKinnon, and L. H. Greene, Phys. Rev. B **35**, 8843 (1987).

[12] S. L. Herr, K. Kamarás, C. D. Porter, M. G. Doss, D. B. Tanner, D. A. Bonn, J. E. Greedan, C. V. Stager, and T. Timusk, Phys. Rev. B **36**, 733 (1987).

[13] M. S. Sherwin, P. L. Richards, and A. Zettl, Phys. Rev. B **37**, 1587 (1988).

[14] J. P. Falck, A. Levy, M. A. Kastner, and R. J. Birgeneau, Phys. Rev. B **48**, 4043 (1993).

[15] P. G. Radaelli, J. D. Jorgensen, R. Kleb, B. A. Hunter, F. C. Chou, and D. C. Johnston, Phys. Rev. B **49**, 6239 (1994).

[16] For a recent review, see D. C. Johnston, F. Borsa, P. C. Canfield, J. H. Cho, F. C. Chou, L. L. Miller, D. R. Torgeson, D. Vaknin, J. Zarestky, J. Ziolo, J. D. Jorgensen, P. G. Radaelli, A. J. Shultz, J. L. Wagner, S.-W. Cheong, W. R. Bayless, J. E. Schirber, and Z. Fisk, in *Phase Separation in Cuprate Superconductors*, edited by E. Sigmund and K. A. Müller (Springer-Verlag, Heidelberg, 1994), pp. 82–100.

[17] R. J. Birgeneau and G. Shirane, in *Physical Properties of High Temperature Superconductors I*, edited by D. M. Ginsberg (World Scientific, Singapore, 1989), p. 198.

[18] J. H. Cho, F. Borsa, D. C. Johnston, and D. R. Torgeson, Phys. Rev. B **46**, 3179 (1992), and references therein.

[19] F. C. Chou, F. Borsa, J. H. Cho, D. C. Johnston, A. Lascialfari, D. R. Torgeson, and J. Ziolo, Phys. Rev. Lett. **71**, 2323 (1993).

[20] P. G. Radaelli, J. D. Jorgensen, A. J. Shultz, B. A. Hunter, J. L. Wagner, F. C. Chou, and D. C. Johnston, Phys. Rev. B **48**, 499 (1993).

[21] C. Chaillout, S-W. Cheong, Z. Fisk, M. S. Lehmann, M. Marezio, B. Morosin, and J. E. Schirber, Physica C **158**, 183 (1989); C. Chaillout, J. Chenevas, S-W. Cheong, Z. Fisk, M. Marezio, and B. Morosin, *ibid.* **170**, 87 (1990).

[22] J. D. Jorgensen, B. Dabrowski, S. Pei, D. G. Hinks, L. Soderholm, B. Morosin, J. E. Schirber, E. L. Venturini, and D. S. Ginley, Phys. Rev. B **38**, 11 337 (1988).

[23] J.-C. Grenier, N. Lagueyte, A. Wattiaux, J.-P. Doumerc, P. Dordor, J. Etourneau, M. Pouchard, J. B. Goodenough, and J. S. Zhou, Physica C **202**, 209 (1992); J.-C. Grenier, A. Wattiaux, J.-P. Doumerc, P. Dordor, L. Fournes, J. P. Chaminade, and M. Pouchard, J. Solid State Chem. **96**, 20 (1990).

[24] E. Takayama-Muromachi, T. Sasaki, and Y. Matsui, Physica C **207**, 97 (1993).

[25] D. C. Johnston, F. Borsa, J. H. Cho, F. C. Chou, D. R. Torgeson, D. Vaknin, J. L. Zarestky, J. Ziolo, J. D. Jorgensen, P. G. Radaelli, A. J. Shultz, J. L. Wagner, and S.-W. Cheong, J. Alloys Compounds **207/208**, 206 (1994).

[26] J. S. Zhou, H. Chen, and J. B. Goodenough, Phys. Rev. B **50**, 4168 (1994).

[27] F. C. Chou, D. C. Johnston, S-W. Cheong, and P. C. Canfield, Physica C **216**, 66 (1993).

[28] M. Reedyk and T. Timusk, Phys. Rev. Lett. **69**, 2705 (1992).

[29] C. Chaillout, S-W. Cheong, Z. Fisk, M. S. Lehmann, M. Marezio, B. Morosin, and J. E. Schirber, Physica C **158**, 183 (1989).

[30] P. M. Grant, S. S. P. Parkin, V. Y. Lee, E. M. Engler, M. L.

Ramirez, J. E. Vazquez, G. Lim, and R. D. Jacowitz, Phys. Rev. Lett. **58**, 2482 (1987).
[31] A. Wattiaux, J. C. Park, J. C. Grenier, and M. Pouchard, C.R. Acad. Sci. Ser. B **310**, 1047 (1990).
[32] F. C. Chou, J. H. Cho, and D. C. Johnston, Physica C **197**, 303 (1992).
[33] S-W. Cheong, Z. Fisk, J. O. Willis, S. E. Brown, J. D. Thompson, J. P. Remeika, A. S. Cooper, R. M. Aikin, D. Schiferl, and G. Gruner, Solid State Commun. **65**, 111 (1988).
[34] S. Uchida, J. Phys. Chem. Solids **53**, 1603 (1992).
[35] Frederick Wooten, *Optical Properties of Solids* (Academic, New York, 1972).
[36] S. Tajima, H. Ishii, T. Nakahashi, T. Takagi, S. Uchida, M. Seki, S. Suga, Y. Hidaka, M. Suzuki, T. Murakami, K. Oka, and H. Unoki, J. Opt. Soc. Am. B **6**, 475 (1989).
[37] J. K. Kim, I. Bozovic, D. B. Mitzi, and A. Kapitulnik, Phys. Rev. B **41**, 7251 (1990).
[38] R. T. Collins, Z. Schlesinger, F. Holtzberg, and C. Feild, Phys. Rev. Lett. **63**, 801 (1990).
[39] A. Zibold, M. Durrler, A. Gaymann, H. P. Geserich, N. Nucker, V. M. Burlakov, and P. Müller, Physica C **193**, 171 (1992).
[40] C. C. Homes, T. Timusk, R. Liang, D. A. Bonn, and W. N. Hardy, Phys. Rev. Lett. **71**, 1645 (1993).
[41] C. Y. Chen, R. J. Birgeneau, M. A. Kastner, N. W. Preyer, and T. Thio, Phys. Rev. B **39**, 11 563 (1989).
[42] K. Kamarás, S. L. Herr, C. P. Porter, N. Tache, D. B. Tanner, S. Etemad, T. Venkatesan, E. Chase, A. Inam, X. D. Wu, M. S. Hegde, and B. Dutta, Phys. Rev. Lett. **64**, 84 (1990).
[43] D. van der Marel, H-U. Habermeier, D. Heitmann, W. König, and A. Wittlin, Physica C **176**, 1 (1991).
[44] M. Mostoller, J. Zhang, A. M. Rao, and P. C. Eklund, Phys. Rev. B **41**, 6488 (1990).
[45] F. E. Bates and J. E. Eldridge, Solid State Commun. **72**, 187 (1989).
[46] J. L. Servoin, Y. Luspin, and F. Gervais, Phys. Rev. B **22**, 5501 (1980).
[47] K. Kamarás, K.-L. Barth, F. Keilmann, R. Henn, M. Reedyk, C. Thomsen, M. Cardona, J. Kircher, P. L. Richards, and J.-L. Stehlé, J. Appl. Phys. **78**, 1235 (1995).
[48] J. F. Scott, Phys. Rev. B **4**, 1360 (1971).
[49] W. E. Pickett, R. E. Cohen, and H. Krakauer, Phys. Rev. Lett. **67**, 228 (1991).
[50] A. P. Litvinchuk, C. Thomsen, and M. Cardona, in *Physical Properties of High Temperature Superconductors IV*, edited by D. M. Ginsberg (World Scientific, Singapore, 1994), p. 375.
[51] I. Ohana, M. S. Dresselhaus, Y. C. Liu, P. J. Picone, D. R. Gabbe, H. P. Jenssen, and G. Dresselhaus, Phys. Rev. B **39**, 2293 (1989).
[52] S. Sugai, Phys. Rev. B **39**, 4306 (1989).
[53] M. Čopič, D. Mihailovič, M. Zgonik, M. Prester, K. Biljaković, B. Orel, and N. Brničević, Solid State Commun. **64**, 297 (1987).
[54] K. F. McCarty, J. E. Schirber, S.-W. Cheong, and Z. Fisk, Phys. Rev. B **43**, 7883 (1991).
[55] C. Thomsen and M. Cardona, in *Physical Properties of High Temperature Superconductors I*, edited by D. M. Ginsberg (World Scientific, Singapore, 1989), p. 509.
[56] P. Böni, J. D. Axe, G. Shirane, R. J. Birgeneau, D. R. Gabbe, H. P. Jenssen, M. A. Kastner, C. J. Peters, P. J. Picone, and T. R. Thurston, Phys. Rev. B **38**, 185 (1988).
[57] I. Bozovic, K. Char, S. J. B. Yoo, A. Kapitulnik, M. R. Beasley, T. H. Geballe, Z. Z. Wang, S. Hagen, N. P. Ong, D. E. Aspnes, and M. K. Kelly, Phys. Rev. B **38**, 5077 (1988).
[58] S. Etemad, D. E. Aspnes, M. K. Kelly, R. Thompson, J. M. Tarascon, and G. W. Hull, Phys. Rev. B **37**, 3396 (1988).
[59] T. Timusk and D. B. Tanner, in *Physical Properties of High Temperature Superconductors I*, edited by D. M. Ginsberg (World Scientific, Singapore, 1989), p. 339.
[60] G. A. Thomas, in *Proceedings of the Thirty-Ninth Scottish Universities Summer School in Physics of High-Temperature Superconductivity*, edited by D. P. Tunstall and W. Barford (Adam Hilger, Bristol, 1991), p. 169.
[61] D. B. Tanner and T. Timusk, in *Physical Properties of High Temperature Superconductors I*, edited by D. M. Ginsberg (World Scientific, Singapore, 1992), p. 363.
[62] D. A. Bonn, A. H. O'Reilly, J. E. Greedan, C. V. Stager, T. Timusk, K. Kamarás, and D. B. Tanner, Phys. Rev. B **37**, 1574 (1988).
[63] T. Timusk and D. B. Tanner, Physica C **169**, 535 (1990).
[64] J. Orenstein, G. A. Thomas, A. J. Millis, S. L. Cooper, D. H. Rapkine, T. Timusk, L. F. Schneemeyer, and J. V. Waszczak, Phys. Rev. B **42**, 6342 (1990).
[65] C.-X. Chen and H.-B. Schüttler, Phys. Rev. B **43**, 3771 (1991).
[66] A. Moreo and E. Dagotto, Phys. Rev. B **42**, 4786 (1990).
[67] D. Poilblanc, Phys. Rev. B **44**, 9562 (1991).
[68] A. M. Tikofsky, R. B. Laughlin, and Z. Zou, Phys. Rev. Lett. **69**, 3670 (1992).
[69] M. Jarrell, J. K. Freericks, and Th. Pruschke, Phys. Rev. B **51**, 11 704 (1995).
[70] T. Holstein, Phys. Rev. **96**, 535 (1954); Ann. Phys. (N.Y.) **29**, 410 (1964).
[71] P. B. Allen, Phys. Rev. B **3**, 305 (1971).
[72] In conventional strong-coupling metals, such as lead, a Holstein sideband due to electron-phonon coupling has been observed in the normal state infrared spectra. See R. R. Joyce and P. L. Richards, Phys. Rev. Lett. **24**, 1007 (1970); G. Brändli and A. J. Sievers, Phys. Rev. B **5**, 3550 (1972); and B. Farnworth and T. Timusk, *ibid.* **14**, 5119 (1976) for details.
[73] W. Lee, D. Rainer, and W. Zimmermann, Physica C **159**, 535 (1989).
[74] Z. Schlesinger, R. T. Collins, F. Holtzberg, C. Feild, S. H. Blanton, U. Welp, G. W. Crabtree, and Y. Fang, Phys. Rev. Lett. **65**, 801 (1990).
[75] S. L. Cooper, A. L. Kotz, M. V. Klein, W. C. Lee, J. Giapintzakis, and D. M. Ginsberg, Phys. Rev. B **45**, 2549 (1992).
[76] L. D. Rotter, Z. Schlesinger, R. T. Collins, F. Holtzberg, and C. Feild, Phys. Rev. Lett. **67**, 2741 (1991).
[77] C. M. Varma, P. B. Littlewood, S. Schmitt-Rink, E. Abrahams, and A. E. Ruckenstein, Phys. Rev. Lett. **63**, 1996 (1989).
[78] P. B. Littlewood and C. M. Varma, J. Appl. Phys. **69**, 4979 (1991).
[79] A. Virosztek and J. Ruvalds, Phys. Rev. B **42**, 4064 (1990).
[80] C. T. Rieck, W. A. Little, J. Ruvalds, and A. Virosztek, Phys. Rev. B **51**, 3772 (1995).
[81] P. W. Anderson, Science **235**, 1196 (1987); in *Frontiers and Borderlines in Many Particle Physics*, edited by J. R. Schrieffer and R. A. Broglia (North-Holland, Amsterdam, 1989); Phys. Rev. Lett. **64**, 1839 (1990); Science **256**, 1526 (1992).
[82] V. J. Emery, S. A. Kivelson, and H. Q. Lin, Phys. Rev. Lett. **64**, 475 (1990); V. J. Emery and S. A. Kivelson, Physica C **209**, 597 (1993).
[83] P. Monthoux and D. Pines, Phys. Rev. B **49**, 4261 (1994).
[84] D. B. Romero, C. D. Porter, D. B. Tanner, L. Forro, D. Mandrus,

L. Mihaly, G. L. Carr, and G. P. Williams, Phys. Rev. Lett. **68**, 1590 (1992).

[85] G. A. Thomas, D. H. Rapkine, S. L. Cooper, S-W. Cheong, and A. S. Cooper, Phys. Rev. Lett. **67**, 2906 (1991).

[86] D. B. Romero, C. D. Porter, D. B. Tanner, L. Forro, D. Mandrus, L. Mihaly, G. L. Carr, and G. P. Williams, Solid State Commun. **68**, 1590 (1992).

[87] M. Reedyk, Ph.D. thesis, McMaster University, 1992.

[88] J. W. Allen and J. C. Mikkelsen, Phys. Rev. B **15**, 2952 (1977).

[89] S. Uchida, H. Eisaki, T. Ito, Y. Nakamura, K. Takenaka, and K. Tamasaku, Jpn. J. Appl. Phys. Ser. **7**, 133 (1992).

[90] S. L. Cooper, D. Reznik, A. L. Kotz, M. A. Kalow, R. Liu, M. V. Klein, W. C. Lee, J. Giapintzakis, and D. M. Ginsberg, Phys. Rev. B **47**, 8233 (1993).

[91] V. J. Emery and S. A. Kivelson, Phys. Rev. Lett. **71**, 3701 (1993).

[92] Xiang-Xin Bi and Peter C. Eklund, Phys. Rev. Lett. **70**, 2625 (1993).

[93] B. Renker, F. Gompf, E. Gering, D. Ewert, H. Rietschek, and A. Dianoux, Z. Phys. B **73**, 309 (1988).

[94] W. Reichard, N. Pyka, L. Pintschovius, B. Hennion, and G. Collin, Physica C **162–164**, 464 (1989).

[95] M. J. Rice, L. Pietronero, and P. Bruesch, Solid State Commun. **21**, 757 (1977).

[96] M. J. Rice, Phys. Rev. Lett. **37**, 36 (1976).

[97] T. Timusk, C. D. Porter, and D. B. Tanner, Phys. Rev. Lett. **66**, 663 (1991).

[98] M. Reedyk, D. A. Bonn, J. D. Garrett, J. E. Greedan, C. V. Stager, T. Timusk, K. Kamarás, and D. B. Tanner, Phys. Rev. B **38**, 11 981 (1988).

[99] P. J. Hirschfeld (unpublished).

[100] D. N. Basov, R. Liang, D. A. Bonn, W. N. Hardy, B. Dabrowski, M. Quijada, D. B. Tanner, J. P. Rice, D. M. Ginsberg, and T. Timusk, Phys. Rev. Lett. **74**, 598 (1995).

[101] G. Aeppli, R. J. Cava, E. J. Ansaldo, J. H. Brewer, S. R. Kreitzman, G. M. Luke, D. R. Noakes, and R. F. Kiefl, Phys. Rev. B **35**, 7129 (1987).

[102] Y. J. Uemura, V. J. Emery, A. R. Moodenbaugh, M. Suenaga, D. C. Johnston, A. J. Jacobsen, J. T. Lewandowski, J. H. Brewer, R. F. Kiefl, S. R. Kreitzman, G. M. Luke, T. Riseman, C. E. Stronach, W. J. Kossler, J. R. Kempton, X. H. Yu, D. Opie, and H. E. Schone, Phys. Rev. B **38**, 909 (1988).

[103] E. J. Nicol, J. P. Carbotte, and T. Timusk, Solid State Commun. **76**, 937 (1990); Phys. Rev. B **43**, 473 (1991).